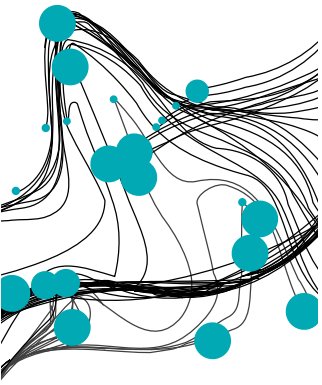

RAM ROBOTICS AND MECHATRONICS

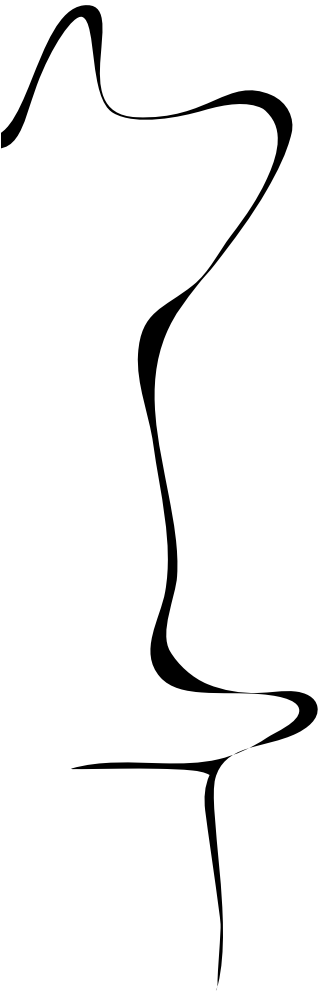

DESIGN AND DEVELOPMENT OF A NEEDLE-PLACEMENT MECHANISM TO MINIMIZE THE NUMBER OF SCANS DURING IMAGE-GUIDED PROCEDURES

R. (Diwakar) Shastri

MSC ASSIGNMENT

Committee:
dr. ir. J.F. Broenink
dr. ir. M. Abayazid
ir. E.E.G. Hekman
ir. S. Neevel
dr. ir. R. Penterman

December, 2020

059RaM2020
Robotics and Mechatronics
EEMCS
University of Twente
P.O. Box 217
7500 AE Enschede
The Netherlands

UNIVERSITY OF TWENTE. | TECHMED CENTRE
UNIVERSITY OF TWENTE. | DIGITAL SOCIETY INSTITUTE

Summary

Percutaneous needle-placement is being extensively employed for clinical procedures like biopsy and ablation. The success of the surgery mainly depends on the accuracy of the needle-placement. Further, the procedure is guided by the feedback provided by imaging devices like Computed Tomography (CT), Magnetic Resonance Imaging (MRI) or Ultrasound (US). Therefore, every needle-placement involves performing multiple scans before placing the needle accurately at the target. Furthermore, procedures like Irreversible Electroporation (IRE), Microwave Ablation (MWA) and Cryoablation involve insertion of multiple needles or probes at the target. This further increases the total number of scans per procedure. This repeated exposure of the patient to hazardous ionizing radiation can cause radiation-induced cancer in the patient.

This report discusses the design and development of a novel device which can perform multiple, accurate needle-placement with minimum number of scans. Various commercially available devices were studied and requirements for the novel device were stated. Based on the requirements different concepts were developed. This study introduces a new category called *ceiling-mounted* devices to assist percutaneous needle-placement. A feasible concept under ceiling-mounted devices was selected. Unlike most of the existing devices, the novel concept requires only two CT scans for the first needle-placement. Subsequent needle-insertion requires one extra scan per procedure to verify the placement. Therefore, with the novel device, n needle-placements require $n+1$ CT scans. Further, the concept was explored and mechanical design of different parts has been discussed followed by kinematic simulations. An estimate of error in the system was calculated and is found to be <2.5 mm for a tumour located at 250 mm depth. Some risks involved in the system were also discussed. A feasibility of the design was verified by analysis against all the requirements. Recommendations for future development were presented.

Contents

1 Introduction

1.1 Background

Minimal-invasive interventions are being extensively used for clinical procedures like biopsy and ablation, due to the advantages they provide over conventional open surgeries, such as shorter hospital stay, reduced tissue damage and faster recovery. The success of the surgery mainly counts on the accuracy of needle placement. Reaching the target with required accuracy is challenging and depends on factors like the size and depth of the tumour with respect to the insertion point. The conventional free-hand needle placement procedure may take multiple iterations and repeated needle manipulation before placing the needle precisely and accurately at the target.

Various needle placement mechanisms ranging from simple passive devices (INRAD, 2020; Beyer et al., 2016; NAV3i, 2020; Medtronic, 2009; NDI-Medical, 2020; Kroes et al., 2013; NeoRad-SimpliCT, 2020; Moser et al., 2013; XACT-Robotics, 2020; Minchev et al., 2017), to sophisticated robots (Arnolli, 2017; Perfint-Healthcare, 2020; Koethe et al., 2014) have been developed to overcome this difficulty and to aid the physician in placing the needle accurately at the tumour. These mechanisms mainly rely on the feedback provided from Computed Tomography (CT), Magnetic Resonance Imaging (MRI) or Ultrasound (US) images. Every needle-placement procedure involves performing multiple scans, to ensure that the needle is placed accurately at the target. However, when second needle insertion is to be made to reach a different tumour located elsewhere in the body, these mechanisms require additional scans to be made and repetition of the whole procedure.

Further, during ablation procedure, it is often required to make multiple needle insertions. From Wells et al. (2015), it can be seen that, in case of Irreversible Electroporation (IRE), at least two probes (electrodes) have to be inserted. If cryoablation is employed, multiple probes are needed to be inserted around the tumour. Furthermore, a major advantage of Microwave Ablation (MWA) over Radio-frequency Ablation (RFA) as stated in Wells et al. (2015) is that, MW has the ability to power multiple probes simultaneously. This means, additional insertions have to be made following the first needle-placement while carrying out ablation procedure.

These additional needle or probe placement requires extra scans to be performed which further exposes the patient to repeated hazardous ionizing radiation, which can lead to radiation-induced cancer in the patient. From the study conducted by Sodickson et al. (2009), it can be noted that 0.7% of baseline cancer incidents are due to CT exposure which contribute to 1% of total mortality due to cancer.

A CT-guided, table-mounted Needle Placement System (Arnolli, 2017) for placing needles in thorax and abdomen region was developed by Demcon Advanced Mechatronics B.V. (DEMCON). However, this Needle Placement System (NPS) also suffers from requiring additional scans to be performed to make a second insertion. Therefore, DEMCON wishes to have a mechanism which enables performing additional insertions without extra scans.

1.2 Goal of the study

The goal of this study is to design and develop a concept for a precise and accurate needle placement device, which also enables the system to perform multiple needle insertions without requiring additional scans for CT guided procedures. This is carried out by studying

commercially available devices and then stating requirements for the novel device. Further, conceptual solutions will be developed to satisfy the requirements and one concept will be selected and further explored by performing a detailed mechanical design. Forward and inverse kinematics will be carried out to study the developed model and the design will be verified against all the requirements by analysis.

1.3 Structure of the report

The structure of this report is as follows: A brief study of literature is presented in Chapter 2. System requirements are stated in Chapter 3. Chapter 4 provides conceptual solutions. Design of individual modules is discussed in Chapter 5. Kinematic simulations are performed and presented in Chapter 6. A verification of design by analysis against all the requirements and limitations of the novel device are discussed in Chapter 7. Finally, Chapter 8 concludes the report along with recommendations.

2 Literature Review

Minimal invasive surgeries are being mainly employed for diagnostic and therapeutic procedures like biopsy and ablation. Accuracy of needle placement plays a crucial role in success of such surgeries. Various devices and mechanisms have been developed to place the needle accurately at the target tumour. In this Chapter, a brief study of free-hand needle placement followed by working principle of existing mechanisms are presented and the accuracy of each type is discussed.

2.1 Conventional Free-hand Needle-Placement

This section mainly discusses the conventional free-hand needle-placement technique. The procedure is carried out in the following manner: the patient is placed on the imager table and general anaesthesia maybe applied. A radiopaque grid is placed on the patient in the region of interest. Initial scanning is performed and the images are obtained. The target tumour is identified in the image and a suitable insertion point is selected such that the needle path does not interfere with impenetrable and critical structures like bones and major blood vessels. It is preferred that the entry point and the target are in the same transversal plane for easy insertion of the needle. Then, the entry point selected in the image is mapped to the patient by moving the CT table to coincide this point with the laser line projected by the laser mounted on top of the CT gantry. The point where the radiopaque grid and the laser beam coincide (illustrated in the Figure 2.1) is marked as the entry point on the skin [ref. (Arnolli et al., 2015)].

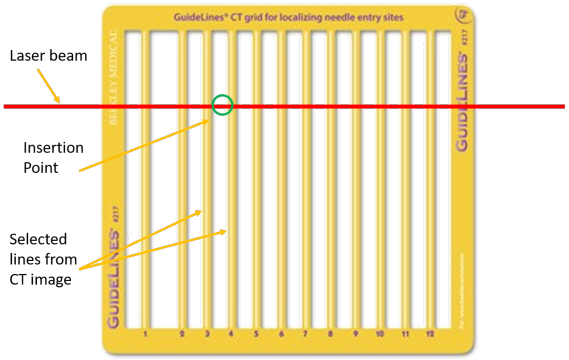

Figure 2.1: Illustration of radiopaque grid placed on patient [ref. GuideLines-CT-Biopsy-Grid (2020)]

The next step in the procedure is to insert the needle, a minor incision maybe made on the skin to facilitate easy insertion of the needle and to avoid tissue damage due to abrupt needle insertion. At this point, the physician should have proper 3D mapping of the patient's body and the exact location of the tumour with respect to the entry point. Depending on one's experience, expertise and risk of damage to the organs in the path, one might choose to insert the needle in one shot or might do it in an iterative method involving intermediate scans to ensure that the needle is indeed in the right path, in which case, the needle is initially inserted superficially and further continued in the same direction or by correcting the angles, based on the feedback from the intermediate scans. The workflow of conventional free-hand needle placement is briefly compiled as a flowchart in the Figure 2.2.

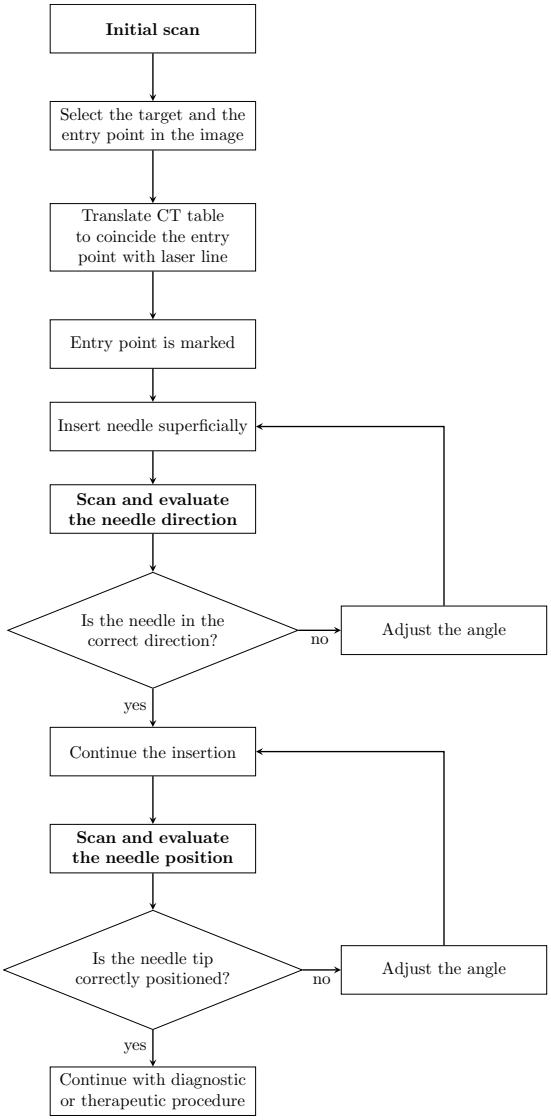

Figure 2.2: Workflow of conventional freehand needle placement (Arnolli et al., 2015)

Furthermore, depending on the target size and location, the complexity and difficulty to reach the target increases. Reaching smaller and deeper targets is more challenging. From Figure 2.2 it can be seen that, depending on the skills of the physician, it takes multiple scans before the needle can be accurately placed at the target. This repeated scanning, insertion and readjustment causes

1. Increased tissue damage
2. More hazardous ionizing radiation exposure to patient.
3. CT being occupied for longer duration (increasing procedural cost and limiting number of patients that can be handled).

Hence, various systems have been developed to assist the placement of the needle.

2.2 Needle Placement Mechanisms

Various systems ranging from simple passive device to sophisticated robots have been developed and are discussed in the literature (Arnolli et al., 2015). They are broadly classified into different categories for ease of understanding as follows:

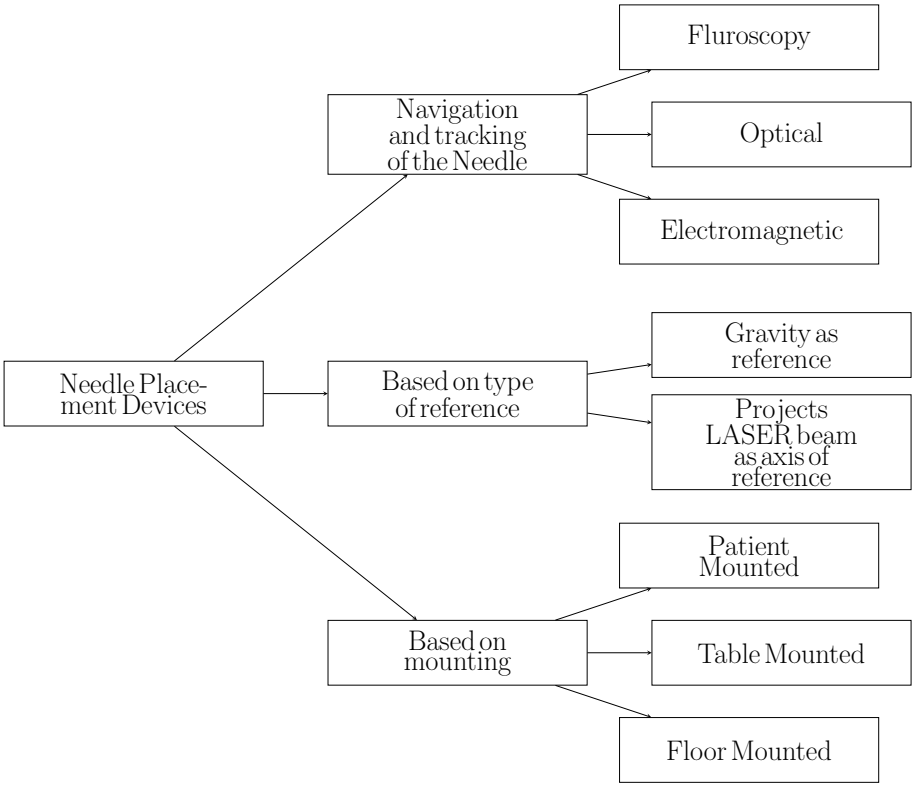

Figure 2.3: Classification of needle placement devices

2.2.1 Navigation and Tracking

In addition to the feedback provided by the CT or MRI, other types of feedback (optical or electro-magnetic) are supplied to the physician to orient and place the needle in correct position. However, these devices do not provide any actuation to orient the needle. The placement and orientation has to be carried out manually. These devices provide real-time feedback about the position and orientation of the needle. The information is presented visually to the physician through graphical representation of images. Based on the type of feedback, this is further classified as:

Fluoroscopy

As a first alternative to free-hand needle placement, a continuous CT fluoroscopy is performed, where the patient is injected with a contrast agent or X-ray dye through intra-venal (IV) means. This allows real-time visualization of the needle path and the target. Although this method provides real-time feedback about relative position of the needle and the tumour, the major drawback of this method is that both patient and the physician are exposed to continuous radiation for nearly 18 minutes during therapeutic procedures in abdominal region (McParland, 1998). However, a lead apron is worn provided to the physician to limit the radiation exposure.

Optical feedback:

This is one of the most widely used methods to obtain feedback in medical navigation. Optical markers are placed in the instruments and on the patient's skin, infrared cameras are used to capture the images and track the needle. Some examples of commercially available systems are

1. CAScination CAS-ONE, Figure 2.4a (CAS-ONE, 2020; Beyer et al., 2016)
2. Stryker NAV3i, Figure 2.4b (NAV3i, 2020)

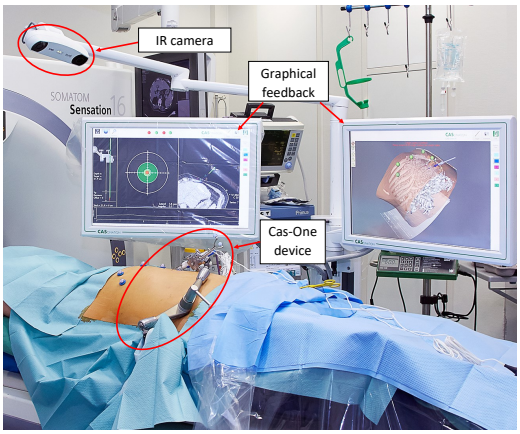

(a) Cascination CasONE adapted from Beyer et al. (2016)

(b) Stryker NAV3i adapted from (NAV3i, 2020)

Figure 2.4: Navigation and Tracking: Optical Feedback Devices

In these devices, the physician has to constantly monitor the screen providing the graphical feedback of the orientation while concentrating on the actually position and placement of the needle guide.

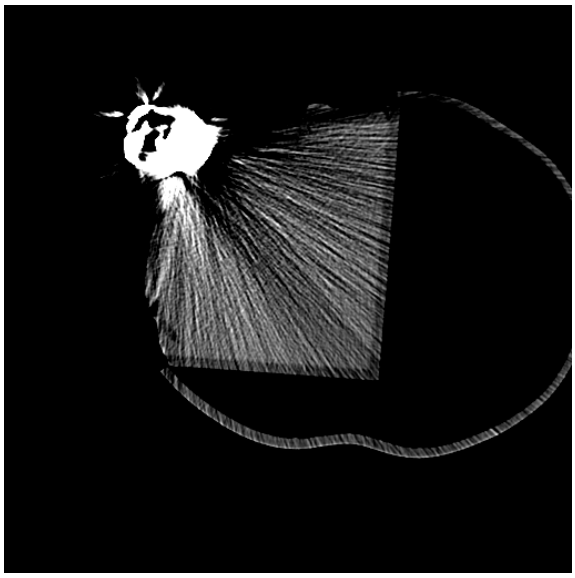

Figure 2.5: CT image of a phantom with CAS-One Cascination device (Shastri, 2019)

During one of the visits to University Medical Center Groningen (UMCG), the author had an opportunity to get a first-hand experience of using *CAScination CAS-ONE* system. It was found during the trial that concentrating on the placement and orientation of needle on the phantom while looking at the graphical feedback was not only challenging but also a tedious and time-consuming process which requires skill and experience. Although these procedures are not intended to be carried out by a novice physician, the procedure should be simple and easy, and should not be distracting the concentration on the main task ie., biopsy or ablation. Furthermore, the device consists of a so-called magic arms which is made of steel. Since the device enters the scanning area for registration scan, a significant amount of metal artefacts can be seen in the image (refer Figure 2.5). The intensity of metal artefacts is higher at the surface of the skin close to the device and gradually decreases. Discussion with the physicians at UMCG revealed that, if the tumour is located close to the skin, the artefacts hinder identifying the location of the tumour.

Also, since in these type of systems, the camera is used to detect the infrared light reflected by the surgical instruments, it requires to be in line-of-sight. This limits the amount of usable space around the patient.

Electromagnetic feedback:

A controlled, changing magnetic field is generated by a generator and an electromagnetic sensor is used to detect and measure the electromagnetic induction. Orientation and position of the needle is deduced from the measured signal. Example devices are

1. Medtronic StealthStation AxieEM (Medtronic, 2009)
2. NDI Aurora (NDI-Medical, 2020)

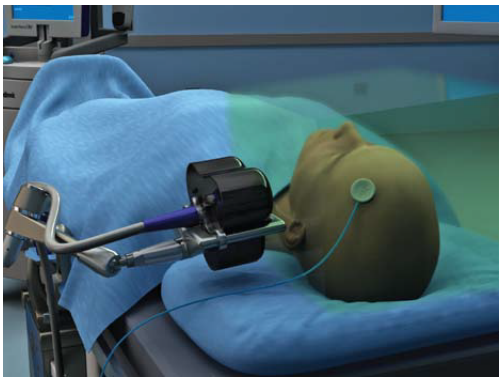

(a) StealthStation AxiEM adapted from Medtronic (2009)

(b) NDI Aurora adapted from NDI-Medical (2020)

Figure 2.6: Navigation and Tracking: Electromagnetic Feedback Devices

Unlike the optical feed-back systems, in these systems a coil is placed on the patient and on the surgical instrument. The relative field strength between these two coils is measured and the position of the needle tip with respect to the other coil placed on the patient is located in the 3D space. Since the EM waves can travel through the objects, these devices do not require to be placed in line-of-sight.

However, the accuracy of the navigation and tracking highly depends on proper patient registration ie., locating the patient with respect to the device. Further, any displacement or disturbance to the sensor mounted on the patient while cleaning the skin with disinfectant can result in errors, in which case, the patient registration needs to be performed again.

2.2.2 Devices based on reference

Devices that make use of gravity as reference

In these type of systems, the direction of gravity is used as reference to orient the needle. The simplest method is to use a two-dimensional bubble level to align the device parallel to floor and use this reference to orient the needle at right angles. Further, a protractor is used to orient the needle rotation along the axis perpendicular to the floor. This concept is employed in INRAD AccuPlace (Figure 2.7) (INRAD, 2020).

Figure 2.7: INRAD AccuPlace adapted from INRAD (2020)

This device helps in orienting the needle in the right angle. However, a minor disturbance during initial positioning can lead to error. Additionally, this method requires intermediate scans to ensure the direction of the needle.

Projected LASER line as axis of reference:

LASER lines are projected along the planned trajectory of the needle path and the needle is placed at the point where the LASER beam touches the skin. The hub of the needle is then aligned with the LASER beam to orient the needle. Some commercially available systems which employ this technique are

1. NeoRad SimpliCT (Figure 2.8a) (NeoRad-SimpliCT, 2020)
2. Amedo Laser Navigation System (LNS) (Figure 2.8b) (Moser et al., 2013)

(a) SimpliCT device, the angles are fed to the system using the knob on the device adapted from NeoRad-SimpliCT (2020)

(b) Amedo LNS adapted from Moser et al. (2013)

Figure 2.8: Laser guided needle placement devices

The former device, SimpliCT requires the physician to manually feed the angles deduced and calculated from the CT scan images to the device and then move the device to coincide the laser beam with the insertion point. However, in the latter device, Amedo LNS uses a user interface which can be connected to any standard CT machine. The insertion point and the target are selected in the user interface. The laser pointer automatically moves to an appropriate position along the circular track around the patient and projects the laser beam on to the insertion point at the correct angle to reach the target.

In both the cases, the physician makes a minor insertion and aligns the needle along the laser beam and further places the needle while trying to keep the needle aligned with the laser beam.

2.2.3 Devices based on mounting

Patient mounted devices

These systems are placed directly over the patient's body and they provide direct physical guidance to the needle guide. This kind of system has an advantage over other systems, that the tissue damage can be reduced, assuming that the topical movement of the patient's body is in coherent motion with that of the target. This assumption is dependent on factors like the depth of tumour from the surface of the body and also the region of interest on the body. However, since this kind of system is placed on the patient and also enters the imaging field, it requires the system to be light weight and made of CT safe materials.

(a) NeoRad Simplify adapted from Kroes et al. (2013)

(b) Apriomed SeeStar adapted from Kroes et al. (2013)

(c) XACT Robotics adapted from XACT-Robotics (2020)

Figure 2.9: Patient mounted needle placement devices

A: Angle and length calculated on the screen; B: Illumination of the intended needle path as seen during the control scan; C: Verification scan after needle placement

Figure 2.10: Illumination of of intended needle path of the Apriomed Seestar in the CT image adapted from Magnusson et al. (2005)

Some examples of commercially available patient mounted devices are

1. NeoRad Simplify (Figure 2.9a)
2. Apriomed Seestar (Figure 2.9b)
3. XACT Robotics (Figure 2.9c)

The workflow of Neorad Simplify for example, involves intermediate scans to be performed to verify and manipulate the needle path. This repeated needle manipulation causes tissue damage. However, in case of AprioMed SeeStar, the need for repeated manipulation is eliminated as the device produces artefacts in the CT image as can be seen in Figure 2.10. Furthermore, the former allows for easy disengagement of the needle once the needle is placed but in the latter, the needle cannot be removed without detaching the device from the patient's body.

Table mounted devices

The table mounted devices are attached to the CT table and similar to the patient mounted devices, these devices also enter the imaging field. Hence, these devices also need to be made of materials compatible for imaging field. Further, the insertion point and the tumour have to be redefined in the coordinate frame of the device which requires an additional scan to be performed to register the device and its initial orientation. However, one advantage of such systems is that the device is gross positioned manually and based on the device's actual placement obtained from the registration scan, accurate angles are calculated.

DEMCON Needle Placement System (Arnolli, 2017) is a table mounted, CT guided system developed at DEMCON in collaboration with University of Twente (UT). The NPS consists of mainly 3 parts,

1. The Locking Module (LM)
2. The Locking Module Arm (LM Arm)
3. The Orientation Module (OM)

The Locking Module, as the name suggests, is a subsystem which not only locks the device to the rails but also locks the top and bottom ball joint. The LM consists of a pneumatic-hydraulic

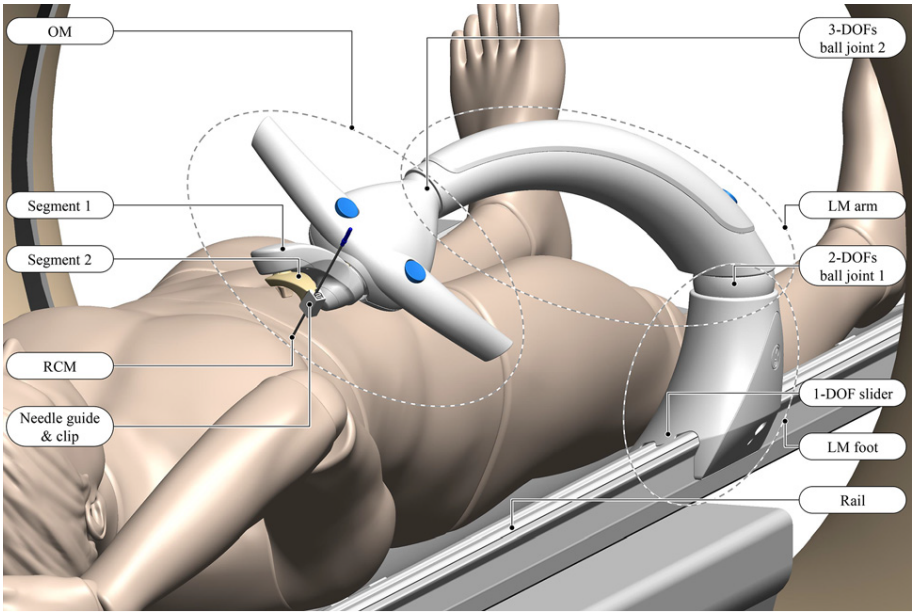

Figure 2.11: Parts of the NPS adapted from Arnolli et al. (2018)

system to generate high locking force. Further, the LM is connected to the Locking Module Arm via *ball joint 1* as shown in Figure 2.11. The LM Arm houses two DC motors to drive the segments. The motors are mounted on cable tensioners. The other side of the LM Arm is connected to the Orientation Module via *ball joint 2*. The OM or the head of the NPS consists of a shaft with two worm wheels, driven by worm. The worm is attached to a pulley which is coupled to the motor with Dyneema cables. The shaft mechanism which consists of two concentric shafts each driving the two segments. The inner shaft is directly coupled to the segment 1 and the outer shaft drives a series of bevel gears to actuate the segment 2. The needle guide is attached at the end of segment 2. Furthermore, in order to define all the points in the same coordinate frame four radiopaque fiducial markers are placed strategically in the NPS. During the device registration scan, the location and relative distance between these fiducial markers are calculated and the orientation of the device is deduced. Exploded view of the NPS is illustrated in the Figure 2.12.

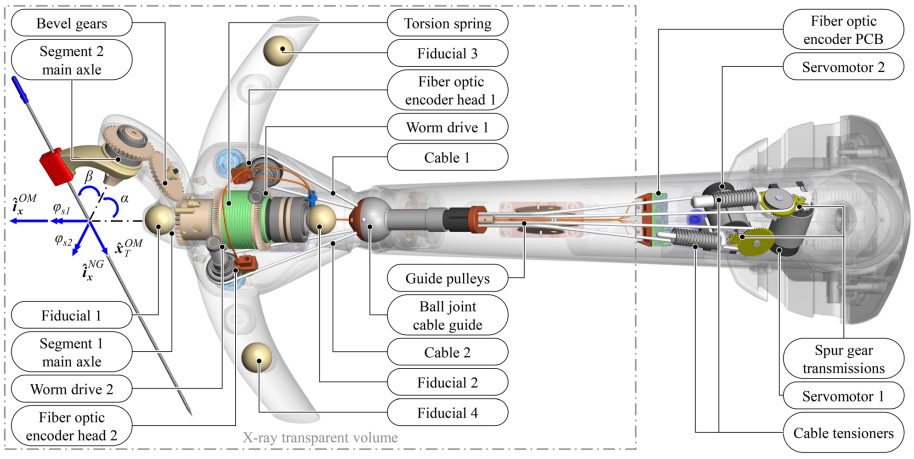

Figure 2.12: Exploded view of the NPS adapted from Arnolli et al. (2018)

Workflow of the NPS

The workflow of the NPS is as follows:

1. The rail is fixed to the CT table.
2. The NPS is placed on the rail.
3. Patient is placed on the CT table.
4. Radiopaque grid is placed on the patient in the region of interest.
5. *Initial (first) scan is performed without NPS in place, to locate the tumour and determine the insertion point.*
6. CT images are evaluated to find the suitable insertion point and the needle path is calculated.
7. CT table is translated to coincide the insertion point with the laser beam projected from the laser mounted on the CT gantry.
8. NPS is positioned appropriately at the insertion point and the OM is locked with respect to the CT table.
9. *Second CT scan is performed.*
10. Image is processed to locate the fiducial markers.
11. Position and orientation of the OM is determined from the images of the fiducial markers.
12. The needle is placed manually by the physician.
13. *Perform third scan to validate the needle placement.*
14. Validate and proceed to therapeutic procedure (biopsy or ablation).

Another example of a similar device is iSYS Medizintechnik (Figure 2.13) (Minchev et al., 2017). The workflow of iSYS is similar to that of DEMCON NPS and requires a device registration scan. However, unlike the NPS, this device can compensate for motion of the target due to respiratory gating.

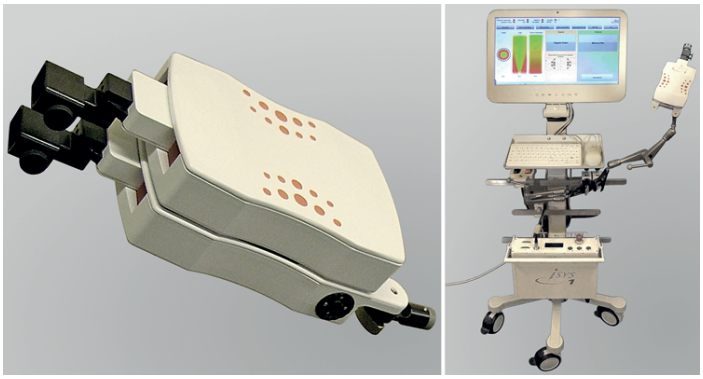

Figure 2.13: Table mounted needle placement devices
iSYS Medizintechnik adapted from Minchev et al. (2017)

Floor mounted devices

Unlike other devices, which move along with the patient, these are mounted firmly to the floor by means of docking station. Hence, these devices do not enter the imaging field and can be made of metals for applications in CT environment. As an advantage over the other type of devices, these systems require one less scan as they do not require device registration and only depend on the initial scan images. This fact also accounts for a disadvantage, since the placement solely relies on the images, there is no more gross positioning of the robot and the initial positioning should be precise and accurate. Thus, these systems require high resolution feedback and well tuned control system to place the needle accurately. Furthermore, the device can occupy a lot of space next to the CT bed creating hindrance to the physician in conducting clinical procedures. However, as an advantage, human error can be reduced significantly due to high resolution encoders and well tuned control system.

Some of the devices are

1. Perfint Maxio (Koethe et al., 2014)
2. Perfint Robio EX

(a) Perfint Maxio **(b)** Perfint Robio EX

Figure 2.14: Floor mounted needle placement devices adapted from Perfint-Healthcare (2020)

2.3 Discussion

Various needle placement mechanisms have been discussed in the previous section. Accuracy of some needle placement mechanisms or devices compared with that of free-hand needle placement is tabulated in the Table 2.1. A number of factors including but not limited to the size of the tumour, depth and angle at which tumour is located with respect to the insertion point, size of the needle; affect the accuracy of placement. Hence, these results are subjected to test conditions. As a standard, every device is compared with free-hand needle placement.

Table 2.1: Accuracy of needle placement of various devices

(All measurements are in mm)

Category	**Device**	**Mean tumour depth**	**Euclidean Error**	**Euclidean Error (free-hand)**	**Reference**
Optical feedback	CasONE (active depth control)	103.6 ± 18.1	4.6 ± 1.3	4.9 ± 1.7	(Wallach et al., 2014)
EM feedback	NDI Aurora	72 ± 25	3.1 ± 2.1	-	(Penzkofer et al., 2011)
Laser guidance	NeoRad SimpliCT	-	0.2	1.2	(Kroes, 2017)
Patient mounted	NeoRad Simplify	-	0.9	1.2	
Table mounted	Medizintechnik iSYS	92.8 ± 14.4	2.3 ± 0.8	-	(Kettenbach et al., 2014)
Table mounted	DEMCON NPS	82.6 ± 25.9	-	14.5 ± 6.4	(Heerink et al., 2019)
		94.8 ± 31.7	9.2 ± 4.0	-	
Floor mounted	Perfint Maxio	110 ± 38	6.5 ± 2.5	15.8 ± 9.2	(Koethe et al., 2014)

2.4 Conclusion

Various needle placement mechanisms are discussed with a brief explanation of their working principle and are broadly classified into different categories. The device either do not provide any physical guidance for needle placement and require multiple intermediate scans followed by repeated needle manipulation which leads to tissue damage like in the case of first two categories. Or, the devices provides physical guidance to the needle guide, however, patient and table-mounted devices also require additional scans to be performed and needs at least three scans per procedure (initial, device registration and verification). For every additional needle placement, required number of scans increases linearly. Every extra scan expose the patient to more harmful ionizing radiation. In floor-mounted systems, device registration scan is eliminated by placing the equipment in a known orientation and at a known position with respect to global coordinates of the gantry.

3 Design Requirements

Requirements for novel needle placement device which enables repositioning of the insertion point is stated in this Chapter. Since the new system is aimed at overcoming the limitations of the DEMCON NPS, requirements for the new system are same as that of the NPS as defined in Arnolli (2017) extended with the ability to reposition and reduce the radiation exposure required for accurate needle placement and in minimum time.

3.1 Primary requirements

Requirement 1: *The system shall be capable of repositioning the end effector to a new entry point with no radiation exposure to the patient.*

Requirement 2: *The system shall be able to place the needle tip at the target within maximum error of* 5 mm *for a target located at a depth of* 250 mm *with a design goal of* 2 mm.

Requirement 3: *The system shall support placement of insertion point in thorax and abdomen region.*

Requirement 4: *The system shall be applicable to needle paths both coincident with and oblique to the transversal plane up to* 90°.

Requirement 5: *The system shall support needles used for biopsy and ablation with diameters ranging between* $14-23$ *gauge.*

Requirement 6: *The system shall support a sterile operating environment.*

Requirement 7: *The system design shall avoid hindrance to the physician by preventing the presence of system components between the patient and the physician.*

4 Conceptual Solutions

Conceptual solutions are developed in this Chapter based on the requirements stated earlier. Advantages and short-comings of the concepts are discussed and at the end of this Chapter, a concept is selected to pursue mechanical design of the system. Furthermore, actuation methods for different joints are briefly studied at the latter part of this Chapter.

4.1 Conceptual Design Solutions

The NPS developed by DEMCON belongs to the table mounted category and requires a device registration scan to be performed to obtain the initial pose of the end effector. The registration of the device is carried out by making a CT scan of the device with the end effector placed at the insertion point on the patient's body. This makes a total of three scans per procedure including the final verification scan. Furthermore, in case a second insertion is to be made, the whole procedure has to be repeated. Therefore, for n needle-placements, NPS requires $2n+1$ CT scans. These additional scans are harmful as they expose the patient to hazardous ionizing radiation. From the study conducted by Sodickson et al. (2009), it can be noted that 0.7% of baseline cancer is due to CT exposure which also accounts for 1% mortality rate due to cancer.

The goal of this Chapter is to develop concept to meet the following requirements:

- Requirement 1: Ability to reposition the end-effector to a new entry point located elsewhere in thorax and abdomen region without extra scan.
- Requirement 3: Ability to place a needle in thorax and abdomen region.
- Requirement 4: Ability to reach a target located coincident with and oblique to transversal plane up to 90°.
- Requirement 7: Ensure minimum hindrance to the physician.

The extra scan for device registration is required mainly due to lack of feedback about the states of intermediate joints and the end effector. Therefore, one of the solutions could be to place encoders on each of the joints. However, since the device contains ball-joints and also due to the limit on overall size of the device (to enable the device to pass through the CT bore), placing encoders is not practical.

Another solution is to rigidly fix the device in known configuration with respect to the patient. This concept was explored and is presented in Appendix A. Although this solves the problem of needing an extra scan, automated repositioning to a different point is not possible, since one of the degrees of motion is constrained due to its fixation to the table. Absolute encoders maybe employed on the rail along with an actuator and locking device. However, if the second needle is to be inserted on the other side of the body, the device has to be relocated to the other side of the CT bed. Therefore, conceptual solutions involving floor mounted system is further explored in this Chapter.

4.1.1 Floor mounted system

Major drawback of a table mounted device is that a translational degree of freedom is lost. By moving the device a step back from table to the floor, the translation of the CT bed can be

exploited to achieve the lost translational degree of freedom. The device is mounted on wheels and by moving the device to lock it to the docking plate fixed to the floor at a known distance from the gantry and the CT table, the device can be made virtually a floor mounted system. This also enables to store the device elsewhere during other clinical procedures.

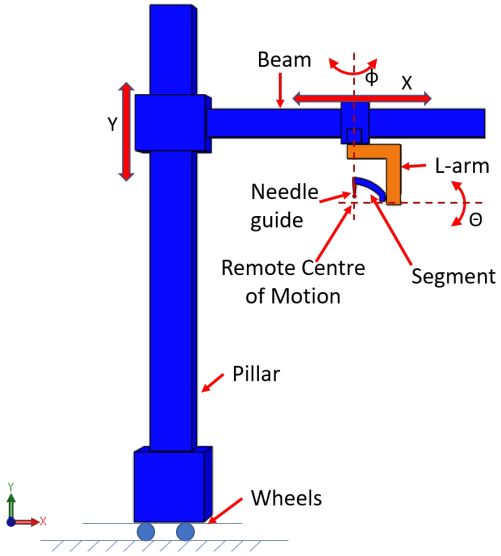

Figure 4.1: Illustration of Concept 2

The device consists of a pillar, a beam, an L-arm and a segment to which needle guide is attached as illustrated in the Figure 4.1. The beam can move along the pillar and the L-arm can move along the beam providing two degrees of translational freedom along X and Y axes. Further, the L-arm can rotate along the vertical axis, Φ, and the segment connected to the L-arm can rotate along the horizontal axis, θ, providing two degrees of rotational freedom along Y and X axes. The translation along Z is achieved by moving the CT bed towards and away from the device. Thus, the device itself has four degrees of freedom and one additional degree of freedom provided by the CT table, making a total of five degrees of freedom. This allows the system to be positioned anywhere in the thorax and abdomen region. The two rotary axes form a gimbal arrangement enabling the needle to be oriented in angles up to 90°.

Further, the patient is placed on the table and the initial scan is performed. The images are analysed and, the insertion point and the target location are identified in the image. Relative angles between the target and the insertion point are calculated. The insertion point defined in the gantry coordinate system is transformed to the device's coordinate. In the conventional method, the CT table is then translated towards the gantry to align with the laser beam. Instead, the CT table is translated away from the gantry and towards the device to a known offset corresponding to the distance of the needle guide, along the table, from the gantry. Then the L-arm is moved along X and Y to place the Remote Center of Rotation (RCR) at the insertion point. Further, the L-arm is rotated along Φ and the segment along θ to align the needle guide with the extrapolated imaginary line connecting the insertion point and the target. The needle is inserted manually and then it is detached from the device. A verification scan is performed to verify the needle placement.

For repositioning of the insertion point or to insert an additional needle for the case of ablation, the verification scan images are analysed in same manner explained above and the RCR is placed at the new insertion point. Needle guide is then aligned along the line connecting the target and the new insertion point by actuating Φ and θ. The needle is inserted and an

additional verification scan is performed. Thus, this concept requires two scans for initial placement and an additional scan for subsequent insertions as compared to the NPS which requires three scans for initial placement and two additional scans for subsequent placements without repeating the entire procedure.

This concept can be realized in two *Configurations* which are discussed in the subsection below. Further, the end effector consisting of the L-arm, segment and the needle guide can be realized in three *Types* which is discussed in following subsections.

Configurations

The floor mounted concept explained in the previous section can be designed in two ways. Translation of the L-arm can be achieved either by (a) having a rigid beam to which a plate is connected. The L-arm is attached to the plate via motor. Thus, moving the plate along the beam moves the L-arm. Or (b) the L-arm can be rigidly mounted to the beam via motor and the beam itself can be moved along the X axis. These two configurations are discussed below.

1. **Configuration 1: Floor mounted - Rigid beam structure** The first configuration is as depicted in the Figure 4.2. The advantage of this configuration is that the beam can be constructed to have a constant stiffness irrespective of the position of the end effector since the beam is rigidly connected to the pillar. However disadvantage being that, a large beam is always hanging above the patient which concerns the safety of the patient.

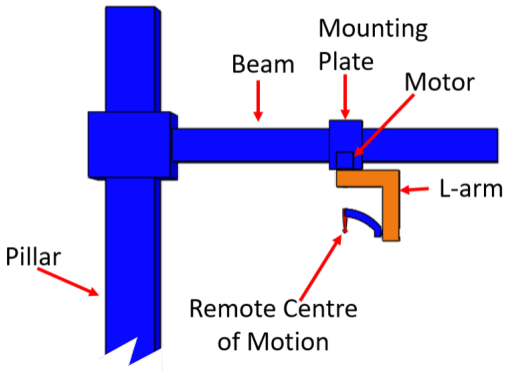

Figure 4.2: Configuration 1: Rigid beam structure

2. **Configuration 2: Floor mounted - Moving beam structure** In the second configuration, the L-arm is attached rigidly to the beam and the beam moves along the X axis as depicted in the Figure 4.3.

   In this configuration, when the beam is at the extreme position, the deflection of the beam is maximum. In the extreme right position of the end effector, the beam deflects downwards as illustrated in Figure 4.4 and for the extreme left position of the end effector, the beam deflects upwards. The value of deflection is directly proportional to the clearance in the linear bearing and inversely proportional to the distance between the two linear bearings.

   This deflection directly affects the accuracy of the system and an error of 92.5 µm can be expected at the needle tip.

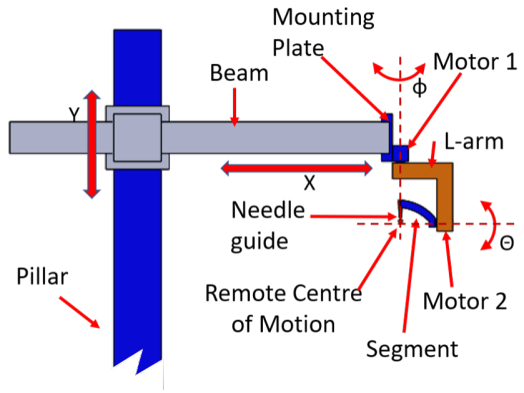

Figure 4.3: Configuration 2: Moving beam structure

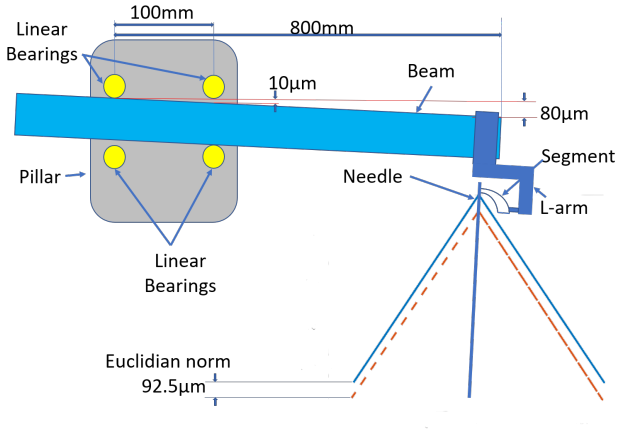

Figure 4.4: Illustration: Error due to deflection of the beam

4.1.2 Ceiling Mounted Device

The downside of floor-mounted systems is that due to the counterweight required to achieve the required stiffness in the beam, the device needs to be heavy. The weight of the device will make mobilizing it difficult. Further a bulky device is placed next to the CT bed, which will hinder the physician while performing the medical procedure. This limitation of a floor-mounted system can be solved by mounting the device to the ceiling. The conceptual idea of a ceiling-mounted device is illustrated in Figure 4.5

Unlike in a floor mounted device, the translation along Y axis happens on the beam. Although in this structure, the beam has to bear comparatively heavier load, the beam is supported at both ends and fixed to the ceiling. Therefore, it can be designed with high stiffness. Furthermore, in a floor mounted system, the device cannot be permanently placed next to the CT bed. Hence, the device needs to be accurately positioned by moving it to a docking station fixed on the floor. A frequent calibration has to be performed to ensure that the device is positioned accurately every time. However, in ceiling mounted system, the device needs to be calibrated only at the time of installation.

Further, ceiling mounted system can be realized in different ways. Conventionally, a lead screw assembly can be employed to achieve the vertical linear motion. However, in the lead screw assembly thus constructed, the carriage of the lead screw should be mounted to the

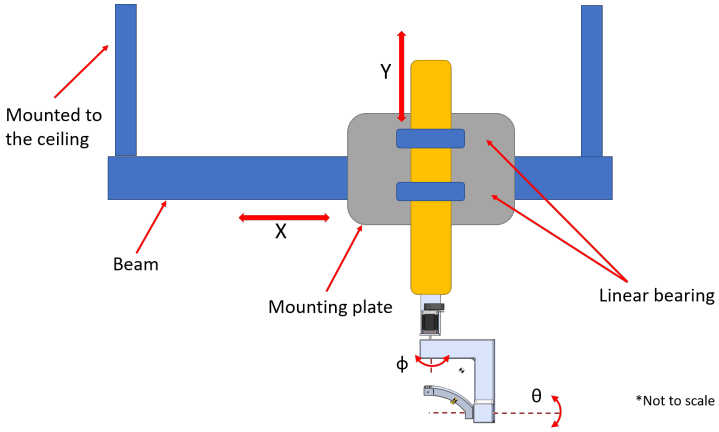

Figure 4.5: Illustration of Concept 3

beam. Instead another configuration can be constructed using a non-captive stepper motor. Unlike a regular stepper motor, a non-captive stepper motor does not contain a shaft. Instead a lead-screw passes through the motor and motor drives a nut. One such motor is shown in the Figure 4.6a. An assembly using such a motor can be realized as illustrated in Figure 4.6b.

(a) Non-captive stepper motor

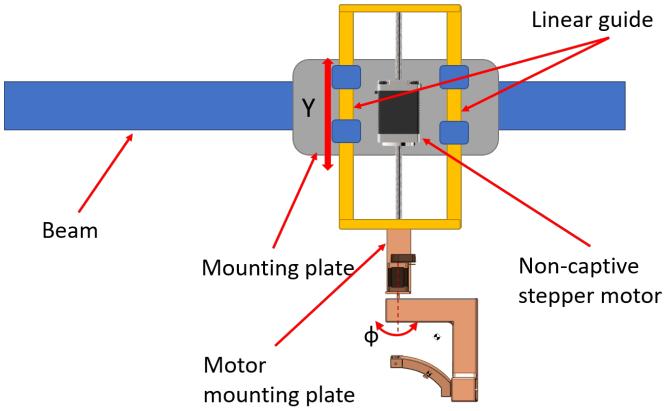

(b) Conceptual diagram using non-captive stepper motor

Figure 4.6

Since there is also rotation along Φ at the end of the assembly, another configuration can be devised to combine both linear and rotational motion. To realize both linear and rotational motion in a single shaft, a *Ball-Screw-Spline* (BSS) shaft can be employed. A ball-spline-screw is a combination of ball-spline shaft and a ball-screw shaft. The shaft is driven by two motors. While one motor actuates the ball-screw nut, the other actuates the ball-spline nut. By turning on only ball-screw motor, the shaft will translate linearly. If ball-spline motor alone is actuated, the shaft assumes a helical motion. If both the motors are actuated in parallel, the shaft rotates along the Φ axis. Therefore, translation along Y and rotation along Φ can both be combined into one single shaft.

(a) Ball-Spline-Screw

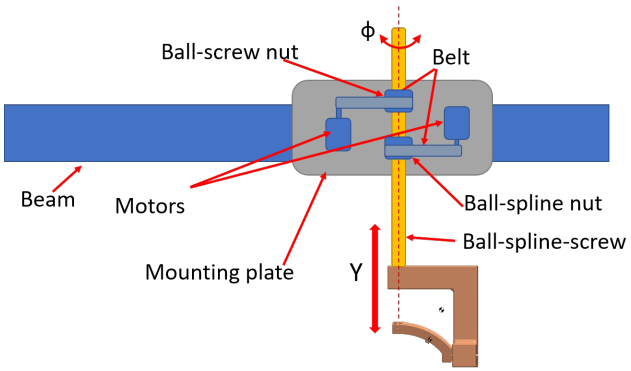

(b) Conceptual diagram using ball-spline-screw

Figure 4.7

4.1.3 Types of end effector

Three types of end effector design can be constructed to achieve Requirement 4, they are:

Type 1: Common RCR

The first type of end effector is as illustrated in the Figure 4.8a. This arrangement has a common RCR. The resulting area of reach is as shown in Figure 4.8b. The radius of each circle corresponds to a particular value of θ and the circumference of each circle corresponds to a particular value of Φ. The cone is constructed for depth of the needle tip from the RCR of 50 mm, 150 mm and 250 mm. Φ is varied from $0 \rightarrow 2\pi$ and θ is varied from $0 \rightarrow \pi/4$. However, θ can be as high as $\pi/2$ and the maximum value of θ is limited for illustration purpose.

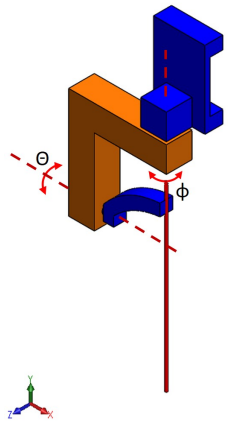

(a) The intersection of the axes is the RCR

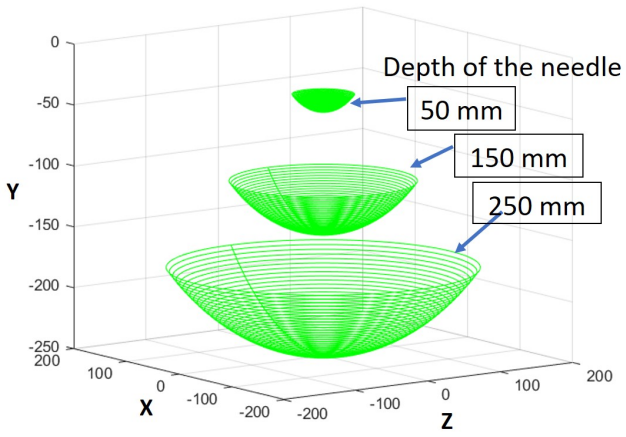

(b) The cone formed by the needle tip for values of θ and Φ

Figure 4.8: Configuration: Type 1

However, for smaller values of θ, the top of the L-arm obstructs the insertion of needle as illustrated in Figure 4.9a. This creates an unreachable zone as shown in Figure 4.9b. One of the solutions is to increase the distance d between bottom of the top part of the L-arm and the top part of the segment, to accommodate for the full length of the needle. However, by increasing d, the overall length of the L-arm increases making it heavier.

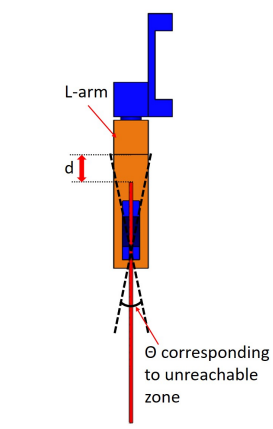

(a) The intersection of the axes is the Remote Center of Motion (RCM)

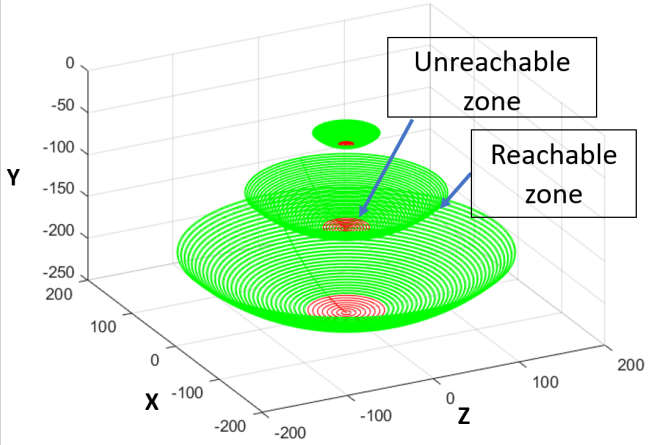

(b) The cone formed by the needle tip for values of θ and Φ

Figure 4.9: Configuration: Type 1 unreachable zone

Type 2: Two RCR

To overcome the limitation of *type 1*, the second type of end effector is developed and is illustrated in the Figure 4.10a. Unlike the previous type, this has two separate RCR for the two axes of rotation. The cone thus formed has a double cone structure as shown in Figure 4.10b. The pink part of the cone is formed for negative angles of θ and the blue part of the cone is formed for the positive angles of θ. The outer cone formed for positive values of θ is larger than the cone formed for *type 1*. This is due to the offset of the axis of rotation of the segment away along the Z plane. Similar to the previous type, Φ is varied from $0 \rightarrow 2\pi$ and θ is varied from $-\pi/4 \rightarrow +\pi/4$.

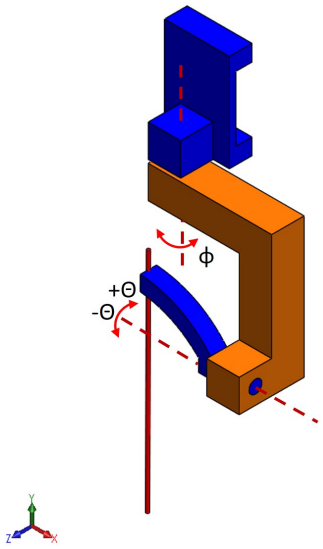

(a)

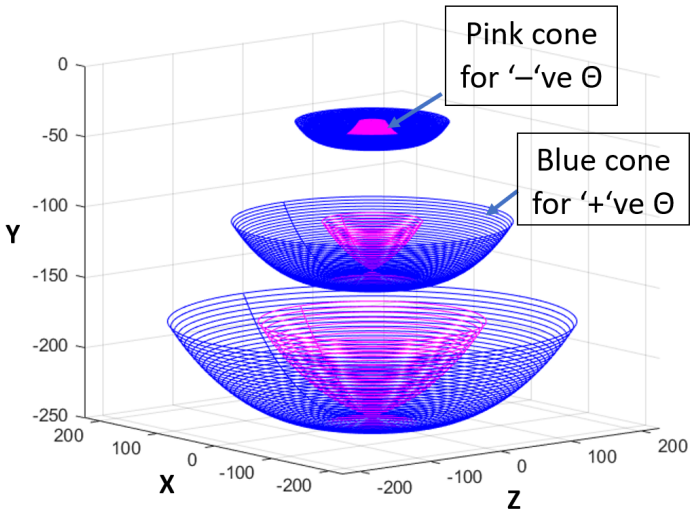

(b) The cone formed by the needle tip for values of θ and Φ

Figure 4.10: Configuration: Type 2

Further, it is apparent that some points cannot be reached due to similar obstruction of the top of the L-arm as illustrated in Figure 4.11a, but, by rotating Φ by π and θ by $\pi/4$, the same

point can be reached from the other side avoiding the obstruction as illustrated in Figure 4.11b. However, since the axes do not have a common RCR, this manipulation involves compensation along X, Y and Z to place the RCR of the segment at the insertion point.

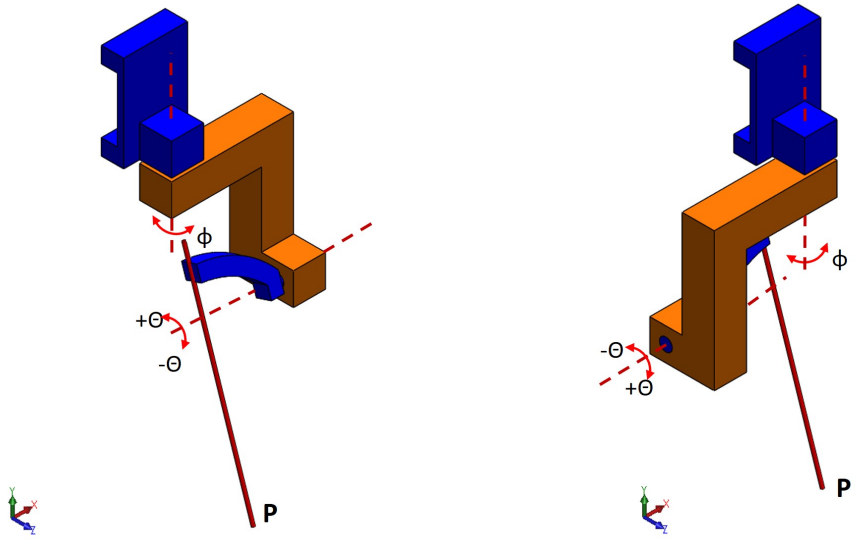

(a) (b)

Figure 4.11: Configuration: Type 2

Formation of double cone is illustrated in Figure 4.12. The axis of rotation of the L-arm is along the axis O depicted in the figure. However, the RCR of the segment is along the axis A at $[-50,0]$ when $\Phi = 0$ and along the axis B at $[+50,0]$ when $\Phi = \pi$. The vertical axis of the plot corresponds to the distance of the needle tip from RCR. The plot shows trace for three needle lengths corresponding to 50 mm, 150 mm and 250 mm from RCR. The graph is plotted for $-\pi/4 \leq \theta \leq \pi/4$ corresponding to RCR at $\Phi = 0$ and $\Phi = \pi$. The region to the right of axis A corresponds to negative values for θ and for $\Phi = 0$. Similarly, the region to the left of axis B corresponds to negative values of θ for $\Phi = \pi$. The pink cone in Figure 4.10b is a resultant of overlapping of two cones in the region corresponding to negative values of θ.

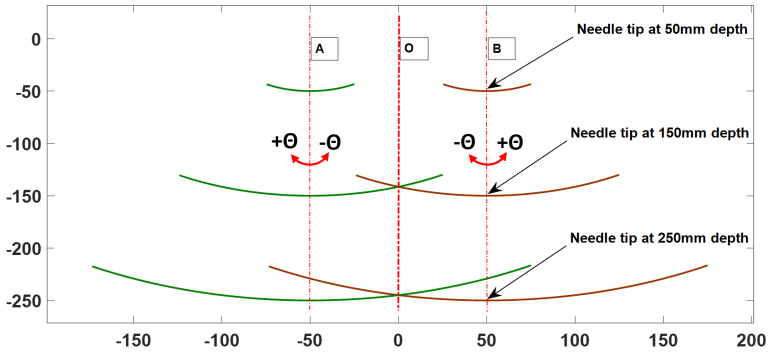

Figure 4.12: Formation of double cone

Further, unlike *type 1*, this arrangement has one-to-many mapping of points. This is illustrated in Figure 4.13. For example, the trace of the needle tip corresponding to needle length of 230 mm from A ($\Phi = 0$) intersects with the trace of the needle tip corresponding to

length of 250 mm from B ($\Phi = \pi$) at point P. That is, the point P can be approached from both the RCR of the segment at A ($\Phi = 0$) and B ($\Phi = \pi$) as illustrated by the dotted lines blue and green. However, in case of approach from B, the needle has to traverse a length of 250 mm inside the patient while in the approach from A the needle has to travel only 230 mm. Although it is wise to choose the approach from A due to its advantages such as reduced needle deflection, reduced tissue damage and easier insertion as the point is very close to transversal plane, this arrangement also provides an alternate approach from B, in case of any obstruction in the path leading from A. Similarly for point Q and any other such points where the needle can be approached from both the RCRs.

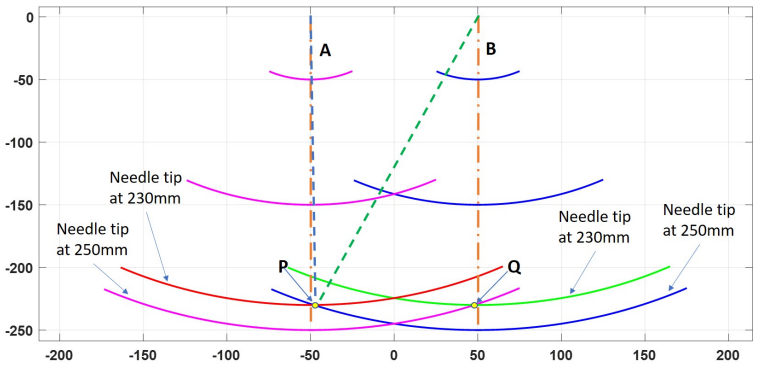

Figure 4.13: One-to-many mapping in type 2

Type 3: Two RCR simplified

The motivation for the L-arm was to have a common remote centre of rotation to both the axes, like in the *type 1*. However, due to the unreachable zone formed by the *type 1*, *type 2* was developed, in which the axis of needle is offset from the axis of Φ. Therefore, *type 2* can be simplified as shown in Figure 4.14a.

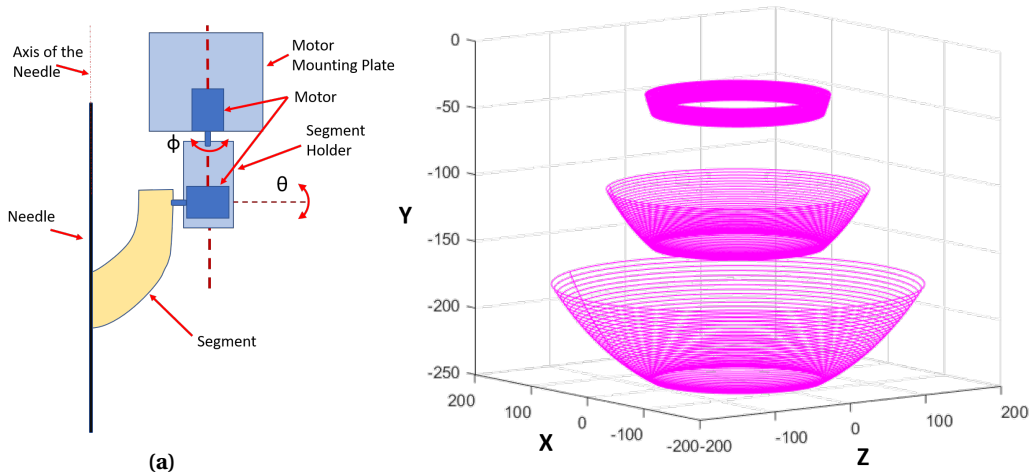

Figure 4.14: Configuration: Type 3

Although from the Figure 4.14b it seems to have some unreachable zones, unlike in *type 1* this region is accessible by repositioning the Φ axis.

Furthermore, since the motor for actuating the segment is placed at the far end of the L-arm, the off-centred inertia in the L-arm is higher, which causes a moment about point A (refer Figure 4.15a). This moment induces an error of 21 µm at the needle tip as illustrated in Figure 4.15b.

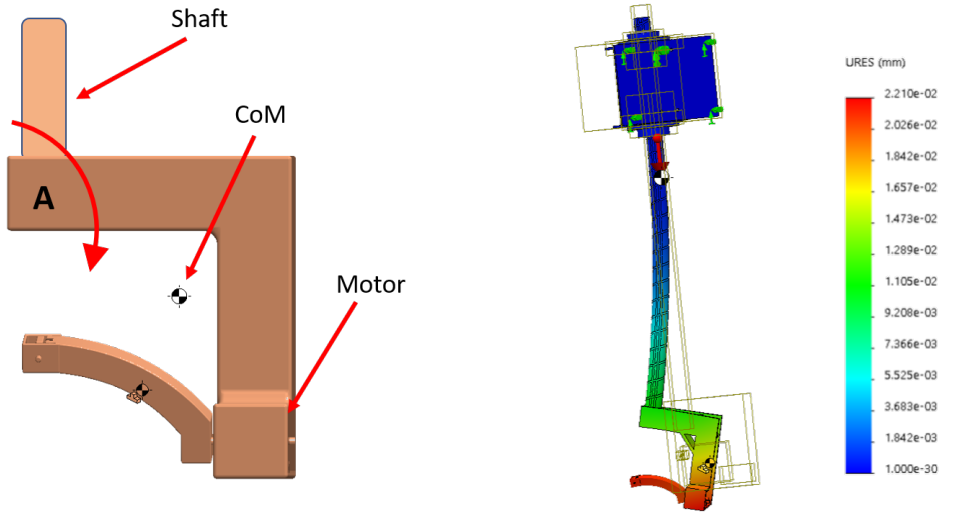

(a) Illustration of moments in L-arm **(b)** Simulation illustrating the moment

Figure 4.15: Error due to moment in L-arm

The advantage of *type 3* design is that, the construction is simple and the off-centred inertia is less compared to that of the L-arm since, the motor for actuating the segment is placed in-line with the axis of rotation of Φ. Therefore, this reduces the error at the needle tip enabling the system to achieve higher accuracy.

4.1.4 Discussion

Four concepts have been developed namely:

1. *Floor mounted; rigid beam*
2. *Floor mounted; moving beam*
3. *Ceiling mounted; non-captive stepper motor actuated*
4. *Ceiling mounted; BSS actuated*

Although these concepts were developed to enable repositioning without performing an additional scan, the floor-mounted concepts are bulky due to the counterweight that is required on the pillar side to keep the overhang stiff enough to meet the Requirement 2, even when the end effector is at the extreme position. This also limits the length of the beam which in-turn reduces area of reach in the thorax and abdomen region.

Considering a case where two tumours are to be targeted and they are located on either side of the body, it would require the device to be moved and repositioned on to the other side of the CT bed. Also, when the device is positioned next to the table, due to its bulkiness the device might hinder the physician's movement in conducting diagnostic or therapeutic procedure.

Therefore, the ceiling mounted systems were conceptualized. Two designs (using a non-captive motor and BSS actuated) have been discussed in ceiling mounted systems. The concept with BSS actuator is further pursued due to its ergonomics and simplicity in construction.

Furthermore, three types of end effector configurations were discussed. The L-arm was mainly developed to have a common remote centre of rotation for both the axes. However, with the feasibility study performed to analyse the reachable area with respect to the insertion point, it was noted that the tumours located within a small angle cannot be reached. To compensate for this, a second type was developed. However, due to the self-weight of the L-arm, a moment is generated which induces an error at the end point. To keep the error minimal, type 3 end-effector configuration is further pursued in this study. Although at the first sight it seems like there is an unreachable zone in this configuration, the region can be reached by repositioning along translational axes. Also, mechanical design and manufacturing of this arrangement is simple and cost effective when compared to the L-arm.

Workflow of the novel device

The work flow of the novel *Ceiling-mounted BSS-actuated* device is presented in Figure 4.16. The workflow of the DEMCON NPS is also presented is Figure 4.17 for easy comparison. From the work flow, it can be seen that image registration scan is eliminated in the novel device.

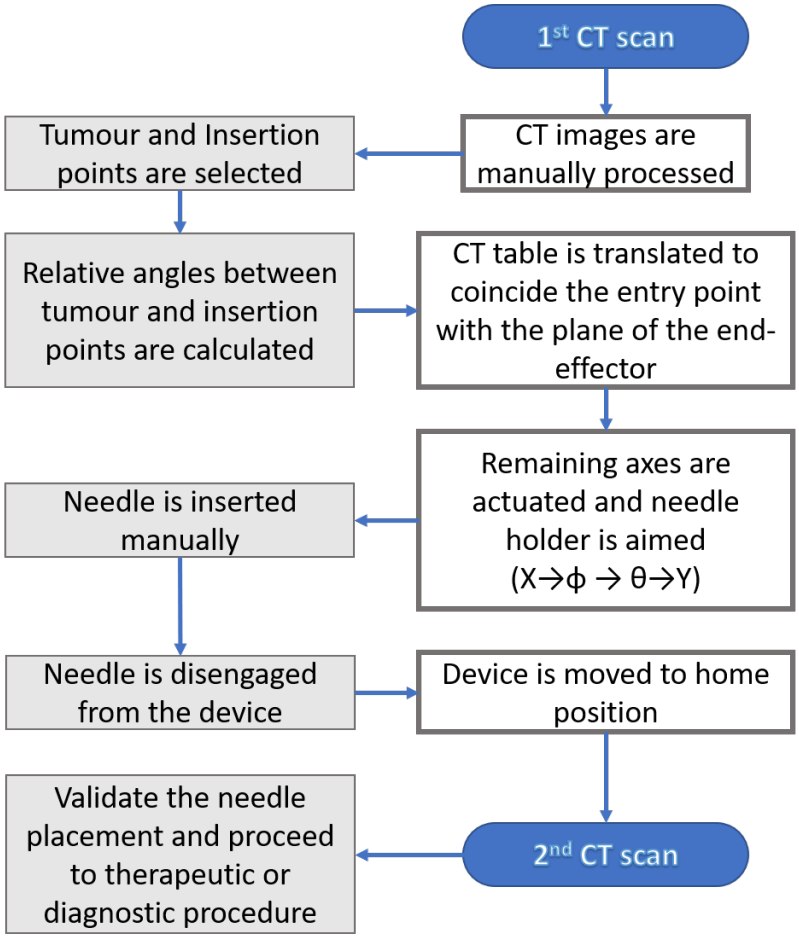

Figure 4.16: Workflow of the novel *Ceiling-mounted BSS-actuated* device

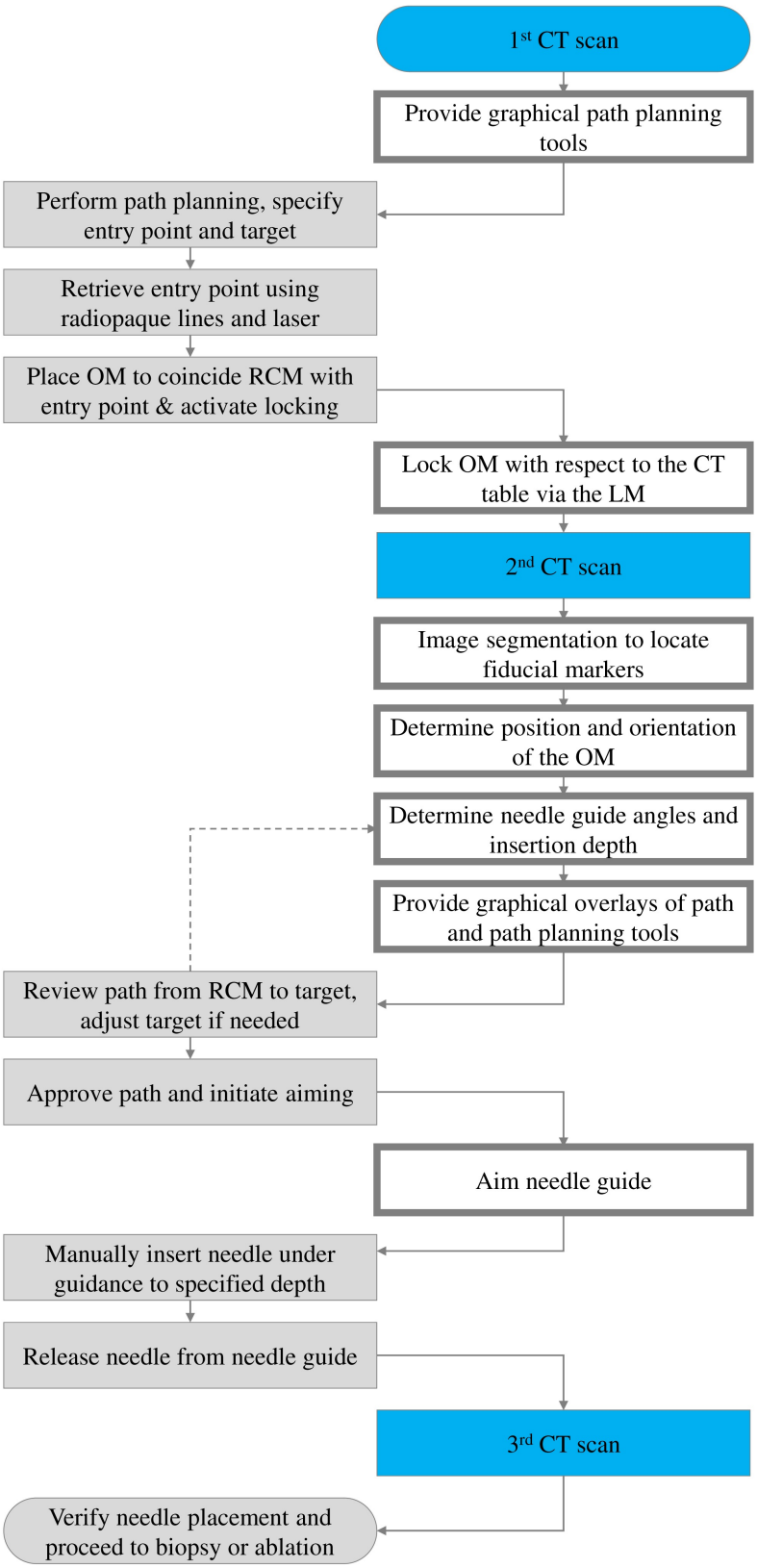

Figure 4.17: Workflow of DEMCON NPS adapted from Arnolli (2017)

4.2 Actuators

Wide range of actuators are available which mainly include electro-magnetic, pneumatic and hydraulic actuators. The simplest being electro-magnetic actuators. The two important types are *DC Servo motor* and *Stepper motor*. The actuator for each joint is further selected based on the requirements in the next section.

4.2.1 DC Motor

DC motors are the simplest and elegant actuators widely used due to its response time and can be controlled accurately. However, if the load is high, intermediate gear reduction is required. The gear box will induce backlash into the system. Furthermore, a DC servo requires relatively sophisticated control system when compared to a stepper motor and requires a very high resolution encoder.

4.2.2 Stepper Motor

Unlike DC motors, stepper motors can drive heavy loads and also have very high holding torque and do not require an intermediate gear reduction stage. Furthermore, stepper motors can be used in open loop and control system is comparatively simpler. A stepper motor has a tolerance of ±5% non-accumulative error. For a typical stepper motor with 400 steps per revolution, maximum error per step will be within 0.09° and this error remains constant for respective step positions. Stepper motors can also be actuated in micro-steps to achieve higher resolution. However, at higher decimation of a step, stepper motor is not reliable in open loop and requires an encoder feedback to ensure the step is reached.

4.3 Drive Systems

The developed concepts involve two translational and two rotational degrees of freedom. One of the two translations and rotations is achieved by the BSS shaft. Actuation mechanism for each joint is briefly conceptualized in this section. Various joints and their respective motion is illustrated in the Figure 4.18

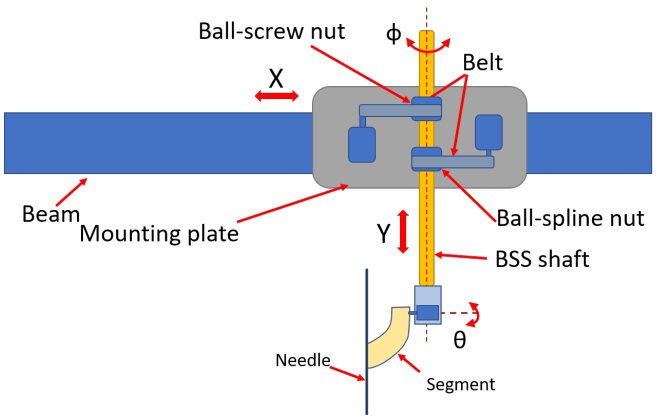

Figure 4.18: Illustration of motion along different axes

4.3.1 Actuation of Segment: rotation - θ

The rotation of the segment can be achieved by directly coupling the motor to the segment so that no non-linearities such as backlash is induced in the system. The segment also requires an active holding torque during the insertion of the needle. The best suitable actuator for this joint is a stepper motor which provides very high holding torque without any gear reduction. By driving the stepper motor in micro-steps, finer angular accuracy can be achieved.

4.3.2 Actuation of BSS shaft: translation - Y; rotation - Φ

BSS shaft involves two nuts that are to be actuated, namely *ball-screw* and *ball-spline*. These nuts can be actuated in two ways, they are,

1. **Geared solution:** A spur gear or a worm gear can be used to drive the nuts using a DC motor. The worm-gear setup also makes the system self-locking. However, by using DC motor and gears, backlash is introduced in the system. An anti-backlash arrangement may be used to eliminate the backlash. By doing so the friction in the system increases and hence a motor with higher driving torque will be required.

2. **Belt drive solution:** Another solution would be to use a belt drive to actuate the nuts. By using a timing-belt and timing-pulley, the slippage in the belt can be eliminated. Furthermore, a stepper motor can be used to actuate the pulley. Due to the advantages like high holding torque and linearity, control of the nut will be simple. Also, by driving the motor in micro-steps, higher accuracy can be achieved.

Belt drive solution actuated by stepper motor is selected for further design due to its simplicity and high holding torque capabilities.

4.3.3 Actuation of Motor-mounting-plate: translation - X

Widely used linear actuators are belt-drive, rack-pinion and a lead-screw. Each drive system has its own advantages and disadvantages. Table 4.1 summarises the performance of each type against important parameters. Due to the advantages like high load driving capabilities, high accuracy and self-locking, a lead-screw system is selected for actuation along the X axis. Since other three joints are being actuated by stepper motor, to maintain uniformity in control systems, the lead-screw is also actuated by a stepper motor.

Table 4.1: Drive system selection table

	Lead Screw	Belt Drive (Timing Belt)	Rack and Pinion
Load driving	High	Moderate	High
Accuracy	High	Low	Moderate
Self-locking	Yes	No	No
Backlash/Slippage (without anti-backlash arrangement)	Yes	No	Yes
Maintenance	Moderate	Low	Moderate

4.4 Conclusion

Of the four concepts discussed, the *ceiling mounted concept with BSS actuated* along with *two RCR simplified* type of end effector configuration is recommended for implementation.

From the workflow of the novel device presented in Section 4.1.4, it can be seen that a CT scan has been eliminated. Further, for repositioning of the end-effector to a new point elsewhere in the thorax or abdomen region, the verification scan from first insertion can be utilized to identify the insertion point and tumour location. Thus requiring one additional verification scan post second insertion. Therefore, for n needle-placements, the novel concept requires $n+1$ CT scans. Further, by designing the stroke for X (refer Figure 4.18) to be as large as width of the CT bed and stroke for Y to reach the CT bed from the ceiling mount, all the points in the thorax and abdomen can be reached since the system also includes movement of CT bed for positioning along Z. Further, the design of end-effector ensures that all angles ≤90° with respect to initial orientation can be achieved. Furthermore, a table-mounted device creates a barrier between the patient and the physician. One should take care not to accidentally hit the device which can disturb the position and orientation of the end-effector. And floor-mounted devices are bulky and occupy a lot of space next to the CT bed limiting the usage space around the patient. However, a ceiling mounted device only extends the end-effector at the insertion point creating very little hindrance to the physician. To ensure that the physician does not accidentally hit his head to the ceiling-mount, the distance from ceiling-mount to floor should be designed to be more than average human height.

Further, various drive mechanisms were presented and actuation of each joint was analysed in detail. Stepper motor is selected as actuator for all the joints due to its high holding torque and high resolution in micro-stepping. Actuation of the segment is achieved by coupling the motor directly to the segment and actuation of BSS shaft is achieved by a belt-drive mechanism. Furthermore, a lead-screw mechanism was selected due to its advantages like high accuracy and high load driving capabilities to actuate the motor-mounting plate along X axis.

5 Mechanical Design

Based on the advantages of the ceiling mounted system, the concept with BSS actuation was selected. A detailed design of individual parts of the system are discussed in this Chapter. The parts which are available off-the-shelf are directly employed in the design. For those parts that are not directly available off-the-shelf, similar parts are bought and modified to meet the requirement. Some custom parts are also designed wherever necessary. Further, selection of actuators and encoders are also discussed at latter part of this Chapter.

5.1 Design of Mechanical Parts

Starting from the needle holder and segment, various parts and components of the device are designed in this section. While the conceptual solution addresses the Requirement 1, Requirement 3, Requirement 4 and Requirement 7; the goal of this design study is to meet the following requirements:

- Requirement 2: Ability to reach a tumour located at 250 mm depth with respect to the insertion point within an error of 5 mm with a design requirement of 2 mm.
- Requirement 5: Ability to accommodate needles of different sizes.
- Requirement 6: To ensure the sterility of the field is not violated.
- Requirement 7: To ensure minimal hindrance to the physician.

5.1.1 Segment and Needle holder

As per Requirement 5, the system should support all needle sizes ranging between 14 and 23 gauge that are used for biopsy and ablation procedure. This corresponds to nominal outer diameter between 2.109 mm and 0.642 mm. In order to accommodate for such a range of diameter, one of the options would be to design a 'V' groove and place the needle in the groove. However, in case of a 'V' groove, the axis of the needle changes for different diameters as illustrated in the Figure 5.1. It can be found that the distance between the centres of maximum and minimum diameter is 0.85 mm. This difference directly translates as error at the needle tip. To overcome this problem, an intermediate needle holder is devised. A needle holder is a component that has a groove corresponding to the diameter of the needle. A custom needle holder is designed to suit different needle gauges as shown in Figure 5.2.

Further, the needle holder assembly consists of the needle holder, a plate, plungers, needle holder clip and a spring as illustrated in Figure 5.3. This arrangement is designed to ensure easy dis-engagement of the needle from the device after placing needle in the patient. The groove in needle holder in combination with the spring force exerted by the plate holds the needle in position against gravity. The spring force is calculated taking into account the friction coefficient of the needle material (stainless steel) and the material of the holder and the plate (aluminium). Plungers are pressed in order to remove the holding force on the needle. The attack angle of the plunger is designed to be 30° with respect to horizontal keeping in mind easy operation by the user. A circlip on the inside limits the plunger from moving out any further. The length of the needle holder is designed to minimize the deflection of the needle during insertion.

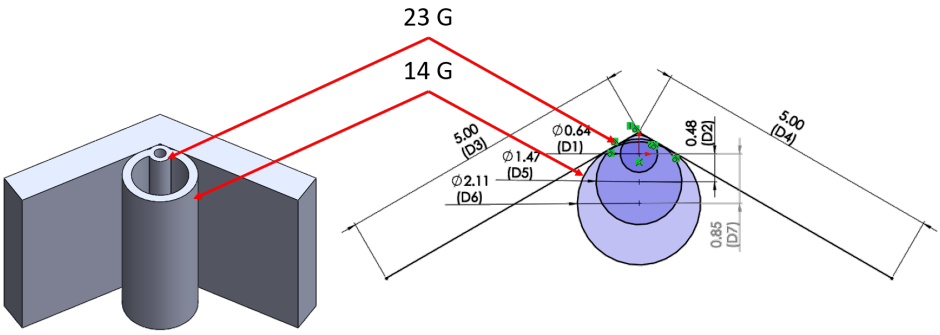

Figure 5.1: Displacement of centre of the needle in v-groove

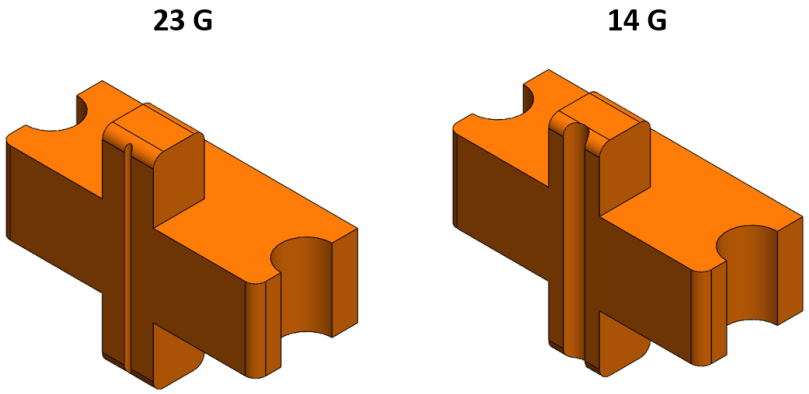

Figure 5.2: Needle holder for gauge 14 and 23 needles.

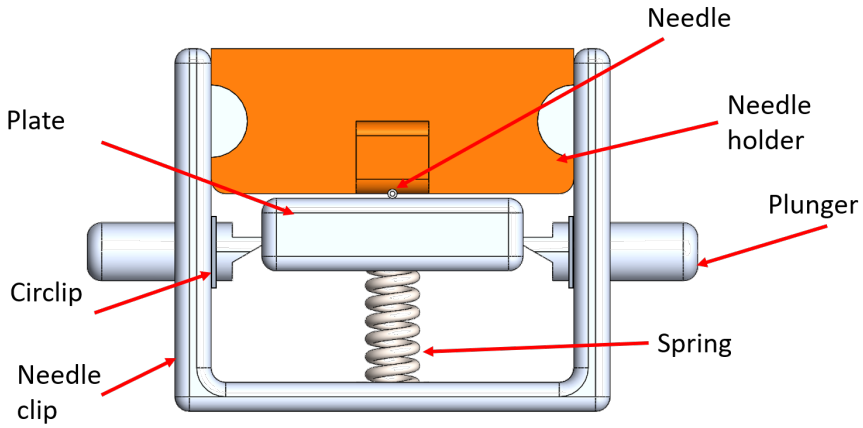

Figure 5.3: Needle holder assembly

The segment is designed to accommodate the needle holder. A counter shape in the segment ensures that the needle holder is properly attached to the segment. An exploded view

of the segment assembly is as shown in Figure 5.4. The inertia of the segment is reduced by removing material by drilling holes on the segment.

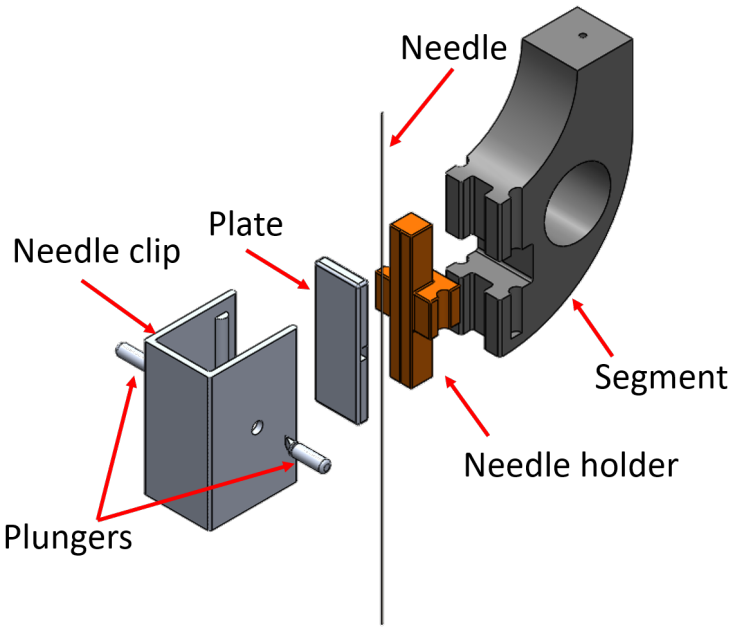

Figure 5.4: Exploded view of the segment assembly

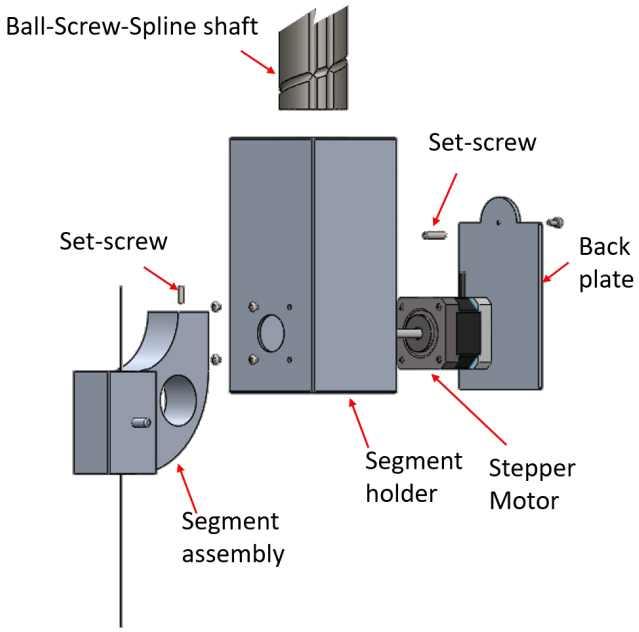

Figure 5.5: Exploded view of segment holder assembly

The segment is coupled directly to the stepper motor. Selection of motor is discussed in the later section of this Chapter. The motor is housed in a segment holder. The segment holder therefore couples the segment to the ball-spline-screw shaft. Exploded view of the segment holder assembly is illustrated in Figure 5.5. To fulfil the Requirement 6, the segment should be

easily removable and sterilizable. The set-screw that couples the motor to the segment enables easy mounting and removal of the segment with the device.

5.1.2 Ball-Spline-Screw (BSS)

The ball-spline-shaft and associated nuts are commercial off-the-shelf parts. The selection of these parts are discussed in this section.

A ball-spline-screw shaft consists of both ball-screw and ball-spline. Two separate nuts, one for ball-screw and other for ball-spline are used to control the position and orientation of the shaft. The mechanism of motion is illustrated in the Figure 5.6. Motors **A** and **B** are coupled to ball-screw and ball-spline nut respectively via timing belts. Actuating ball-screw nut alone will cause the shaft to move linearly and by actuating the ball-spline nut alone will cause the shaft to move in spiral motion (combination of both linear and rotary). However, by actuating both the motors in parallel, shaft will rotate about its axis. With modern-day controllers, actuation and control of two motors in parallel can be easily achieved.

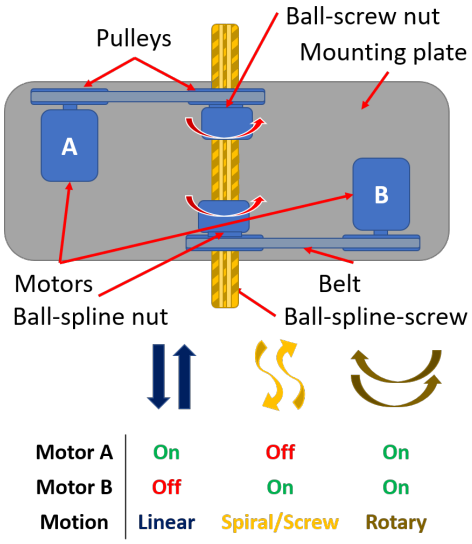

Figure 5.6: Mechanism of motion

The shaft is available as both solid and hollow part. Hollow shaft is selected in this design to keep the weight minimal. The length of the shaft is considered to be 1000 mm. When the force is applied at the end of the shaft to insert the needle, the shaft behaves like a cantilever with a point load at the end. This deflection is calculated using Equation 5.1 and Equation 5.2.

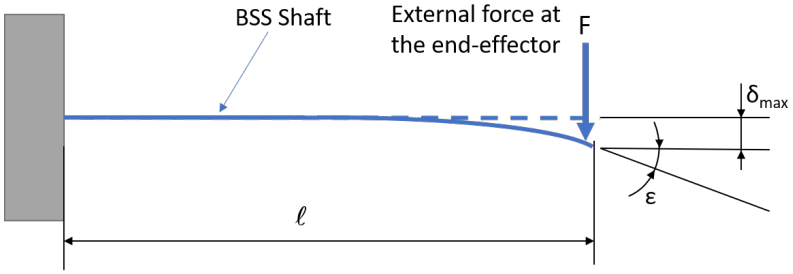

Figure 5.7: Deflection of the beam

$$\delta_{max} = \frac{Fl^3}{3EI} \tag{5.1}$$

$$\epsilon = \frac{Fl^2}{2EI} \tag{5.2}$$

where, δ_{max} is the maximum deflection, F (N) is the force, l (mm) is the length of the overhang, E (N mm^{-2}) is Young's modulus and I (mm^4) is moment of inertia. Maximum deflection and corresponding error at the needle tip considering the angle ϵ is calculated for different diameters of the shaft and tabulated in Table 5.1. The length l =750 mm, E =2.06 × 10^5 N mm^{-2} and force of 25 N is used for the calculation.

Table 5.1: Error in needle placement due to stiffness

Diameter (mm)	I (10^4 mm^4)	δ_{max} (µm)	ϵ (10^{-3} rad)	Error at needle tip $\gamma_{\text{stiffness}}$ (µm)
25	1.51	1130.21	2.260	1695.21
30	3.00	568.87	1.138	853.31
40	9.79	174.32	0.348	261.48
50	25.1	67.99	0.136	101.99

As a trade-off between compact design and stiffness, the shaft with 40 mm diameter is selected for the design.

Furthermore, a scenario similar to Figure 4.4 can be expected since BSS shaft is held at two points and the two nuts are separated by a distance. However, these nuts are preloaded and the clearance for the selected diameter with normal preloading is found to be a maximum of 2 µm [ref. (THK, 2020)] in rotation direction. Considering a maximum of 2 µm clearance, the error at the end of the shaft is found to be 10 µm when calculated for 1000 mm shaft length. However, since angular contact bearing are employed in the nuts and also the length of ball-screw and ball-spline nuts are 98 mm and 100 mm, respectively, the deflection is further reduced and the maximum error at the end of the shaft will be ≤10 µm. This error directly translates to the needle tip. Therefore, maximum error at the needle tip due clearance can be considered as 10 µm. Selected BSS part is listed in Table 5.2.

Table 5.2: Ball-Spline-Screw shaft part

Part name	Ball spline shaft
Part number	BNS4040A-1200L
Manufacturer	THK
Diameter	40 mm
Pitch	40 mm

5.1.3 Motor Mounting Plate Assembly

The motor mounting plate assembly houses the motors to drive the ball-screw-nut and ball-spline-nut. The plate also serves as a coupling between the horizontal lead screw assembly and the ball-screw-spline shaft. The nut holders and motor brackets are manufactured as separate parts and are coupled to the back plate using dowel pins. The centre distance from the drive shaft of the motor to the ball-spline-screw shaft is designed to match the standard length

of the timing-belt. Slots have been provided for mounting the motors (refer Figure 5.8). The belt can be tensioned by adjusting the motor position. The motor-mounting-plate assembly is directly attached to the carriage of the lead-screw assembly.

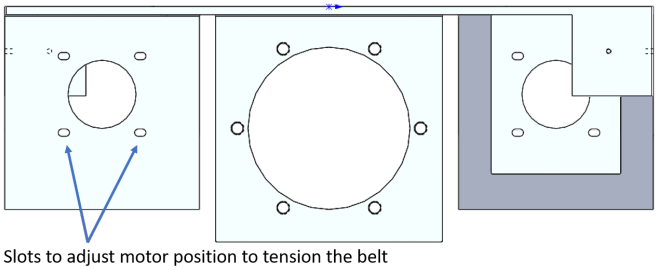

Figure 5.8: Belt tensioning scheme (Top view of motor mounting plate assembly)

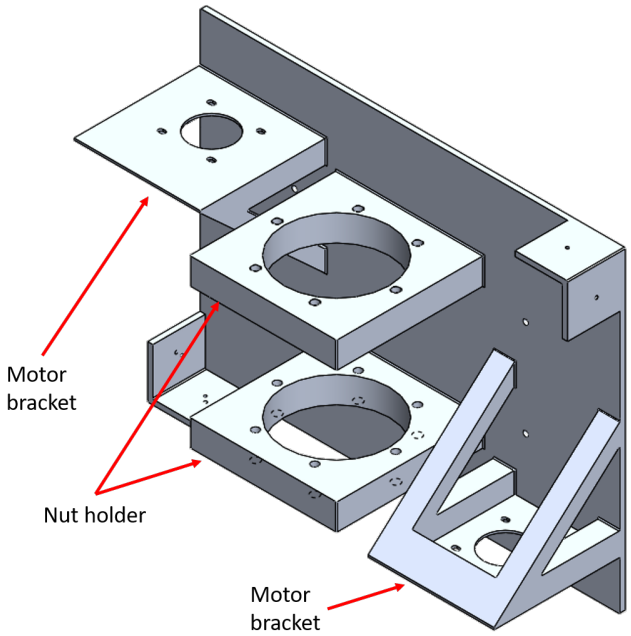

Figure 5.9: Motor mounting plate

5.1.4 Belt and Pulleys

The pulleys are the integral part of the design. Selection of pulley plays a major role in the design. Commercially-off-the shelf pulley is chosen and customised to meet the requirement. The part is made of solid aluminium with steel flanges. The pulley is designed for a T10 timing belt. Correspondingly, a 25 mm width, steel-cable reinforced timing belt is chosen in the design.

For the pulleys that are mounted to the ball-screw-nut and ball-spline-nut, the hub of pulley is machined and the bore is enlarged to accommodate the shaft. The same pulleys are also used for the motors by machining the hub and drilling a hole for set-screw. Customization from the original part is illustrated in Figure 5.10. The selected pulley and belt parts are listed in the Table 5.3.

An exploded view of the motor mounting plate with motors, pulleys, ball-screw and ball-spline nut is as shown in Figure 5.11.

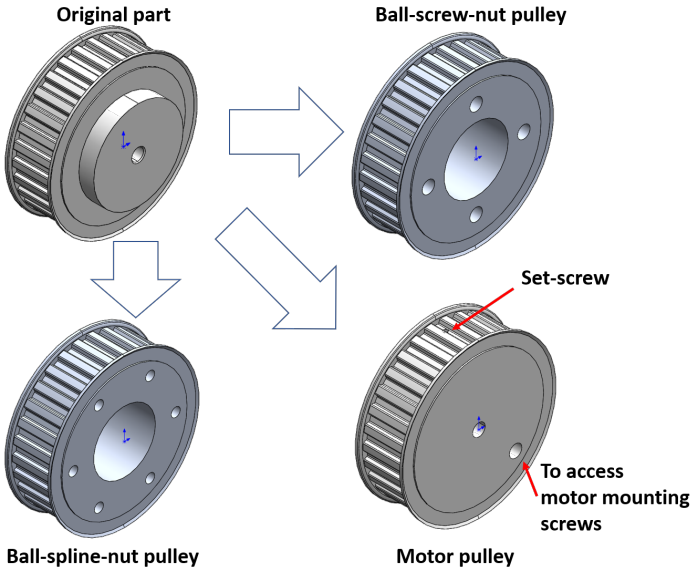

Figure 5.10: Pulleys

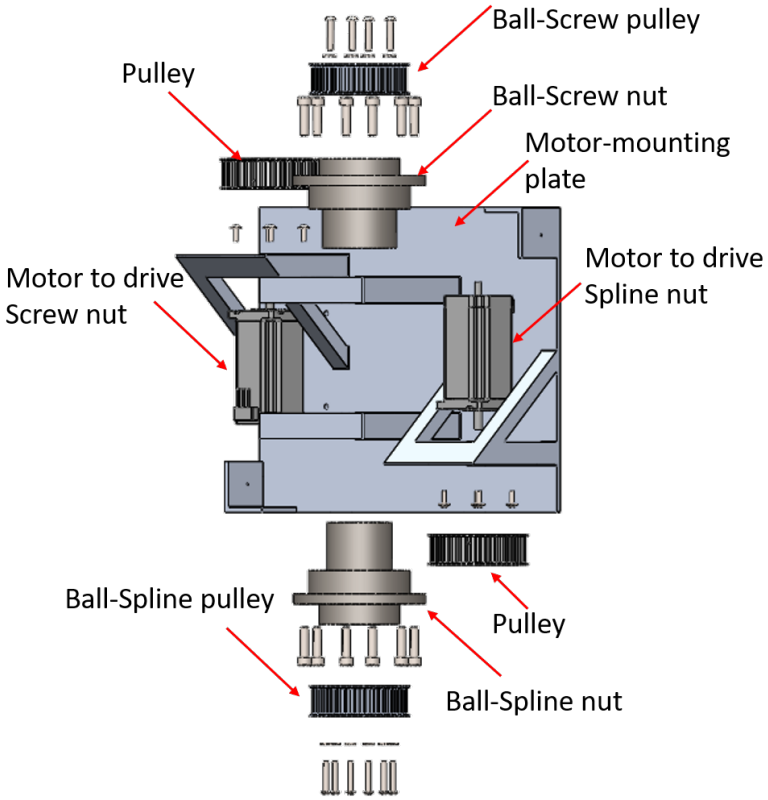

Figure 5.11: Exploded view of motor-mounting plate

Table 5.3: Pulley and Belt part

Part name	**Pulley**	**Belt**
Part number	40T10/30-2	TTBU900T10250
Manufacturer	B&B	Misumi
Pitch Diameter	95.5 mm	-
Tooth style	T10	T10
Material	Aluminium	Polyurethane
Core	-	Steel chord

5.1.5 Lead-screw Assembly

Selection of lead-screw assembly for horizontal displacement of the needle plays a critical role in the design. Various parameters are considered before selecting a proper lead-screw assembly. Firstly, various moments involved in the system are discussed. Moments M_A, M_B and M_C are defined as shown in the Figure 5.12. While M_A and M_C are cause due to the force F_A, M_B is caused due to the force F_B. Required moments for a force of 50 N and rated moments are tabulated in the Table 5.4.

Table 5.4: Moments

Moments	Required	Rated (THK, 2011)
M_A (N m)	4.85	994
M_B (N m)	45.0	994
M_C (N m)	45.0	925

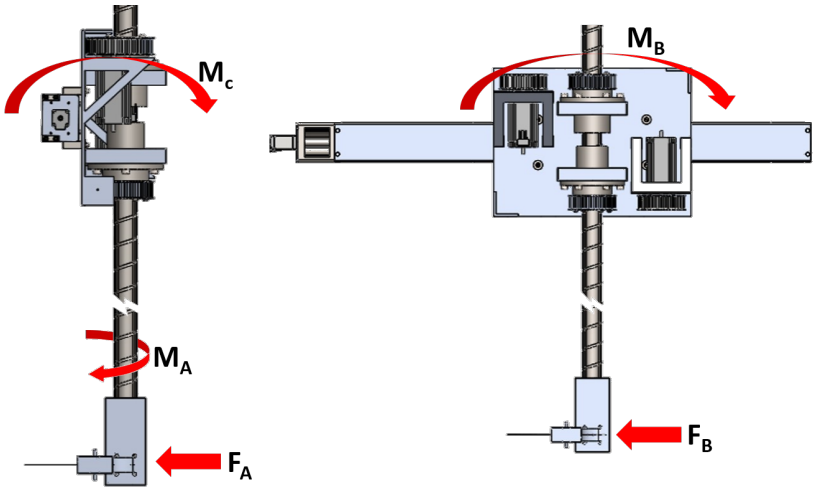

Figure 5.12: Moments in the system

The width and height of the motor-mounting plate is 400 mm × 300 mm. The lead-screw assembly with two short blocks is chosen in the design and are placed at a distance to balance the load. Considering the ball-spline shaft to be rigid, by attaching the motor-mounting plate to two blocks, the effect of M_B and M_A are compensated.

Salient parameters are listed in Table 5.5. From the table, it can be noted that the clearance in the carriage is −0.016 mm, the carriages have angular contact bearings which further reduces

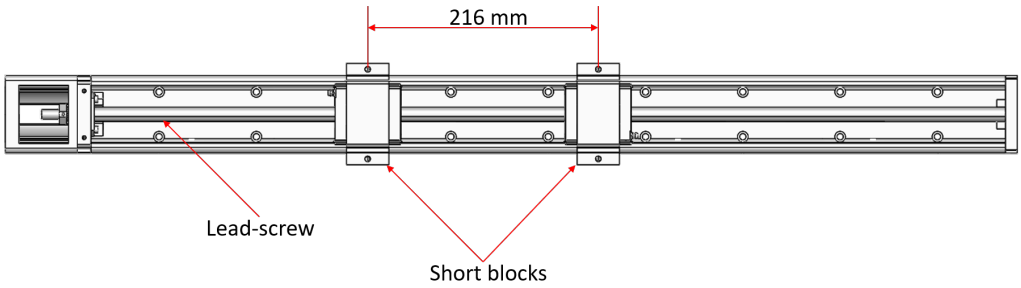

Figure 5.13: Lead-screw assembly

Table 5.5: Characteristics of the lead-screw assembly

LM guide	Basic dynamic load rating (N)	11900
	Basic static load rating (N)	19600
	Radial clearance (mm)	-0.016 to -0.006
Bearing unit (Axial direction)	Basic dynamic load rating (N)	6660
	Static permissible load (N)	3240
Ball Screw unit	Basic dynamic load rating (N)	2940
	Basic static load rating (N)	3720
	Screw shaft dia (mm)	15
	Positioning accuracy (mm)	0.15
	Backlash (mm)	0.02
	Lead (mm)	10

the effect of M_C and the backlash is found to be 20 µm. However, the backlash can be further minimized by pressing the blocks towards or away from each other during the assembly. Selected part is listed in the Table 5.6.

Table 5.6: Lead screw assembly part

Part name	Lead-screw assembly
Part number	KR45H10D+940LH0-100A
Manufacturer	THK

5.1.6 Ceiling mount

Figure 5.15 illustrates the device mounted to the ceiling. Various measurements are also depicted in the figure. Design of ceiling-support is out of scope of this study. However, all the characteristic requirements for the ceiling mount are listed in the Table 5.7. Considering an average human height (in the Netherlands) of 1.8 m, the beam has to be placed at a minimum height of 2 m to the floor to ensure accidental injuries to the physician are avoided. The length of the BSS shaft selected is 1 m considering the CT table height of 1 m from the floor. The clearance above the beam should be a minimum of 1.1 m to ensure enough space for the ball-spline-screw shaft. Therefore, the required ceiling to floor height is 3.1 m. However, from the guidelines stated by Myers (2020), the minimum ceiling height for imaging room is specified as 9'6" which translates to 2.92 m. Therefore, considering the average human height of 1.8 m allows a window of 0.2 m to compromise. By reducing the distance from beam to floor by 0.1 m the stroke-length required by the BSS also reduces by 0.1 m. Therefore, the length of BSS can also be reduced by 0.1 m; or, the beam position with respect to the floor can be retained at

2 m however, a stopper has to be implemented on the BSS shaft to ensure it is not retracted fully resulting in an collision with the ceiling. For the selected LS-assembly, the width of the beam should be a minimum of 1.1 m and distance between the centre of CT bore and the axis of the ball-spline shaft at the extreme position of the device is 345 mm. The distance between gantry and the beam should be strategically selected based on the maximum distance the bed can move from the gantry while also keeping the beam and the device far enough not to cause distortion in CT images. This distance is represented as l in the Table 5.7. Since the X-ray detectors are directional and are placed directly opposite to the transmitter inside the gantry, image will not have any distortions due to any metal outside the gantry region. Therefore, l can be as low as 0 m. However, considering a case where the needle has to be inserted at 60° in sagittal plane with respect to transversal plane as shown in Figure 5.14, it is wise to choose l to be at least 0.75 to 1 m to allow for the physician to stand and operate on the patient.

Weight of the device is approximately 45 kg, considering a maximum of 50 N downward external force on the device the stiffness of the device should be a minimum of 50 kN mm^{-1}. Further, stiffness in other directions should ensure that the maximum deflection is ≤10 µm.

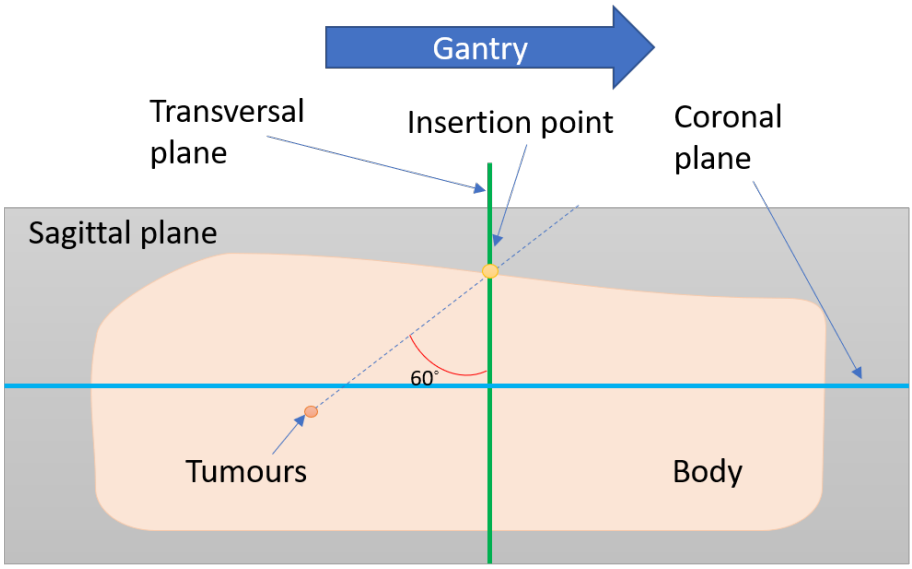

Figure 5.14: Illustration of a case where needle insertion is 60°

Table 5.7: Characteristic features of the ceiling support

Stiffness (kN mm^{-1})	50
h_{device} (mm)	2000
$h_{clearance}$ (mm)	≥1100
w_{beam} (mm)	1100
w (mm)	345.24

5.2 Stepper Motor and Encoder

Selection of motor and its control is a critical aspect in designing high accuracy systems. Actuation methods for different joints was discussed in the previous Chapter. Due to advantages a stepper motor provides such as high holding torque and simple control, stepper motor was selected as actuation mechanism. To achieve high accuracy in positioning, stepper motor has to be driven in micro-stepping mode. Efficiency in positioning of a stepper motor

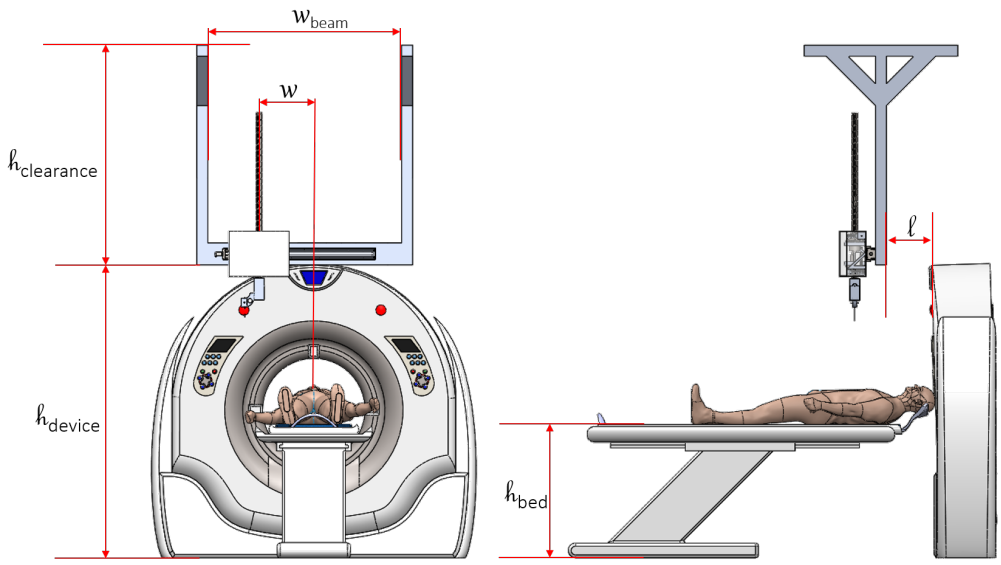

Figure 5.15: Requirements for ceiling mount
CT and Patient models are adapted from (Kandemir, 2015; Cabieses, 2014) respectively

reduces with higher decimation of a step. Although the stepper motor can be driven in open-loop, in order to ensure the motor does not miss steps, an encoder feedback is used and a closed-loop control is employed.

Stepper motors are of three types, *Permanent Magnet* (PM), *Variable Reluctance* (VR) and hybrid stepper motors. The first type, as the name suggests, the rotor is made of permanent magnet and axially magnetized. They offer high torque but low speed. The second type consists of a soft-iron rotor and offer low torque. However, the torque drop at higher speeds is less compared to PM type. A hybrid stepper motor is a combination of both PM and VR and has advantages of both the types. They offer high holding torques and can be operated in micro-stepping mode. Hence, a hybrid type stepper motor is selected in this design.

Stepper motors are further classified into *Unipolar* and *Bipolar*. Different winding types are illustrated in the Figure 5.16. A bipolar stepper motor offers higher torque compared to that of any unipolar configurations since there is only one winding per phase. Driving circuit for a bipolar motor is complex and requires a H-bridge arrangement to reverse the magnetic field. However, with modern day electronics, integrated circuits with built-in H-bridge and free-wheeling diodes are directly available. Due to high torque and higher efficiency compared to a unipolar type, a bipolar motor is selected in this design.

Characteristic requirements for the motors and encoders to actuate different joints are discussed are listed in the Table 5.8. The torque is calculated from the inertia of the part, taken along its axis of rotation and by considering 10% time is required to reach the maximum velocity for angular acceleration. Further, a *Factor-of-Safety* (FoS) of 2 is considered to calculate the required torque. The FoS is considered for all critical parameters.

The selected motors are tabulated with the parametric values in the Table 5.10. Torque speed curves for the three motors are given in Figure 5.17 and encoder parameter are tabulated in Table 5.9.

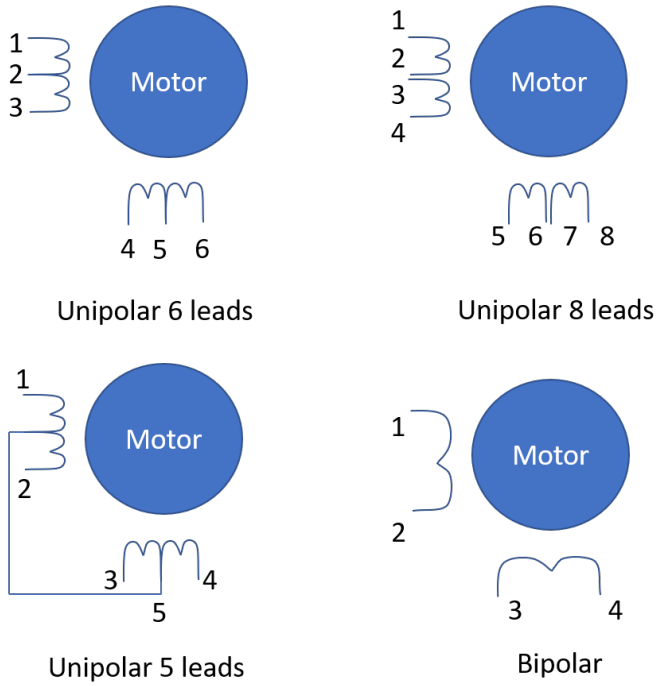

Figure 5.16: Illustration of different types of windings

Table 5.8: Motor and encoder requirements

Joint	Part	Parameter	Required value	Unit
Segment	Motor	Torque (with FoS)	0.004	N m
		Holding torque for 25 N m load (with FoS)	0.365	N m
		Angular velocity	15	RPM
	Encoder	Resolution	4000	PPR
Ball-Screw	Motor	Torque (with FoS)	0.938	N m
		Holding torque for 50 N m load (with FoS)	1.608	N m
		Angular velocity	300	RPM
	Encoder	Resolution	800	PPR
Ball-Spline	Motor	Torque (with FoS)	0.0288	N m
		Holding torque for 50 N m load (with FoS)	1.608	N m
		Angular velocity	15	RPM
	Encoder	Resolution	4000	PPR
LS-Assembly	Motor	Torque (with FoS)	0.16	N m
		Holding torque for 50 N m load (with FoS)	0.238	N m
		Angular velocity	780	RPM
	Encoder	Resolution	400	PPR

Table 5.9: Encoder parameters

Part name	Encoder
Part number	NTO3-05-Z06 (6.35 mm)
Manufacturer	Nanotec
Resolution	5000 PPR

Table 5.10: Motor parameters

Part name	Segment Motor	Ball-Screw Motor	Ball-Spline Motor	LS Motor
Part number	ST4118M0406-B	ST6018D4508-B	ST6018D4508-B	SC3518L1204-B
Manufacturer	Nanotec	Nanotec	Nanotec	Nanotec
Holding Torque	0.396 N m	4 N m	4 N m	0.32 N m
Resolution	1.8°	1.8°	1.8°	1.8°
Type	Bipolar	Bipolar	Bipolar	Bipolar

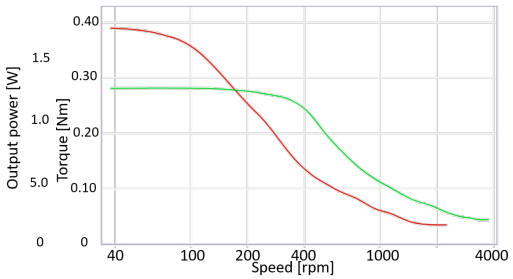

(a) Torque-Speed relation for ST4118M0406-B

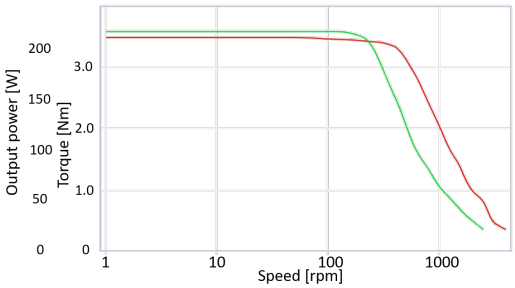

(b) Torque-Speed relation for ST6018D4508-B

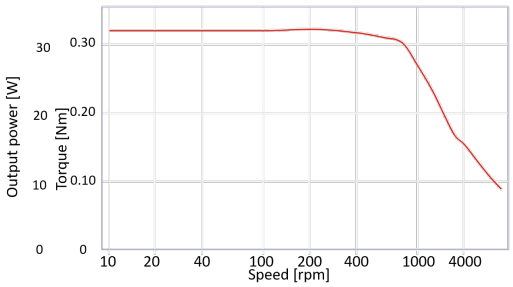

(c) Torque-Speed relation for SC3518L1204-B

Figure 5.17: Torque-Speed curves of the motors
Green: unipolar; Red: Bipolar

5.3 Brakes

The system is mounted to the ceiling and directly placed above the patient. Also, the system consists of the ball-spline shaft. The reverse efficiency of a ball-screw, ball-spline is 95%. Hence it is required that the system should be compensated for gravity. When the system is powered, the holding torque of the motors compensate for both gravity and external loads. However, when the system is turned off, to hold the shaft and end-effector against gravity it is necessary to implement a brake.

Various concepts including applying brake directly on the shaft or on the nuts can be implemented and custom brakes have to be designed for such purposes. The latter idea was explored and is as shown in Figure 5.18. An extension is attached to the nut, a lever is placed such that a linear downward force applied at **A** is amplified and translated as normal force at point **B** (brake shoe - nut interface). Linear force at point **A** can be applied using a solenoid or a captive motor or any other similar linear actuators. Distance to fulcrum from point **A** is designed based on force to stroke ratio of the actuator. The material of the brake-shoe is selected such that the coefficient of friction is maximum. However, designing such a braking

system is a design by itself and is out of scope of this study. Hence, an electric motor brake is employed in this design.

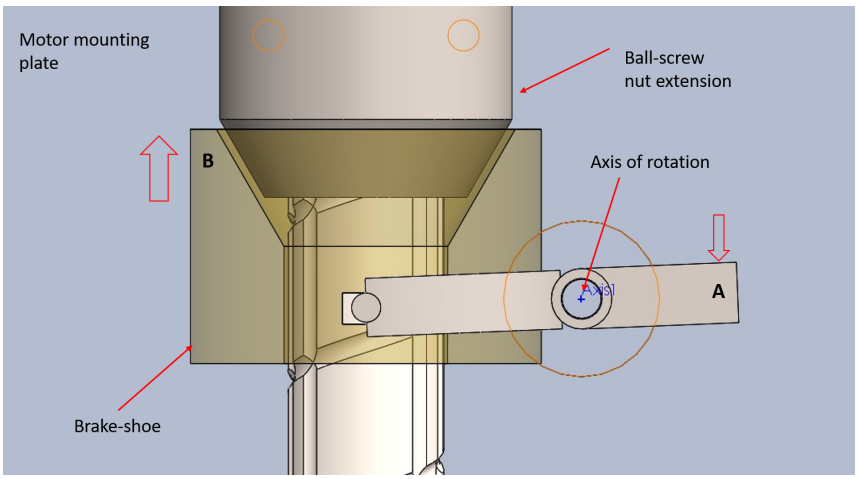

Figure 5.18: Conceptual diagram of braking system

As a simpler option, electric motor brakes can be coupled directly to the shaft of motors actuating ball-screw and ball-spline nuts. A normally **ON** brake is selected in this design, hence brakes have to be powered to disengage the braking force. The reflected torque due to gravity is calculated as

$$\tau_{Brake} = \frac{\{6.5 \times 9.8\}\ (\mathrm{N}) \times 40\ (\mathrm{mm})}{2\pi \times 0.95} = 0.4268\ \mathrm{N\,m}$$

Considering a safety factor of 5 required braking torque is approximately 2 N m. The brake part selected is listed in the Table 5.11.

Table 5.11: Brake part

Part name	Brake
Part number	BKE-2,0-6,35
Manufacturer	Nanotec
Holding torque (N m)	2

5.4 Conclusion

A detailed design on all the parts and components of the system have been discussed in this Chapter. While some parts are custom designed other parts have been bought off-the-shelf and modified (if required) to meet the requirements. Further, components such as motors, encoders, brakes, belts have been selected with a safety factor to ensure smooth and safe operation of the system. The novel *ceiling-mounted, BSS-actuated* device thus developed is shown in Figure 5.19

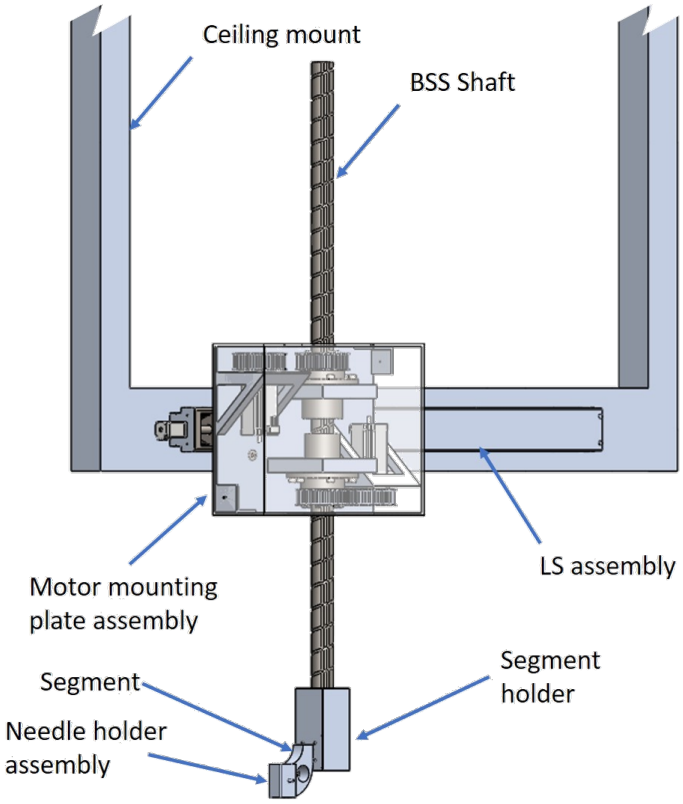

Figure 5.19: Novel device: *Ceiling-mounted, BSS-actuated*

6 Kinematic Simulations

A detailed design of the mechanical system was discussed in the previous Chapter. Forward and inverse kinematics are performed and error analysis of the device is presented in this Chapter.

6.1 Forward Kinematics

Coordinate frames at various points are defined and Homogeneous Transformation Matrix (HTM) are derived in this section. *Left-Posterior-Superior* (LPS) system is employed in the study. Coordinate frames are put at various joints as illustrated in Figure 6.1.

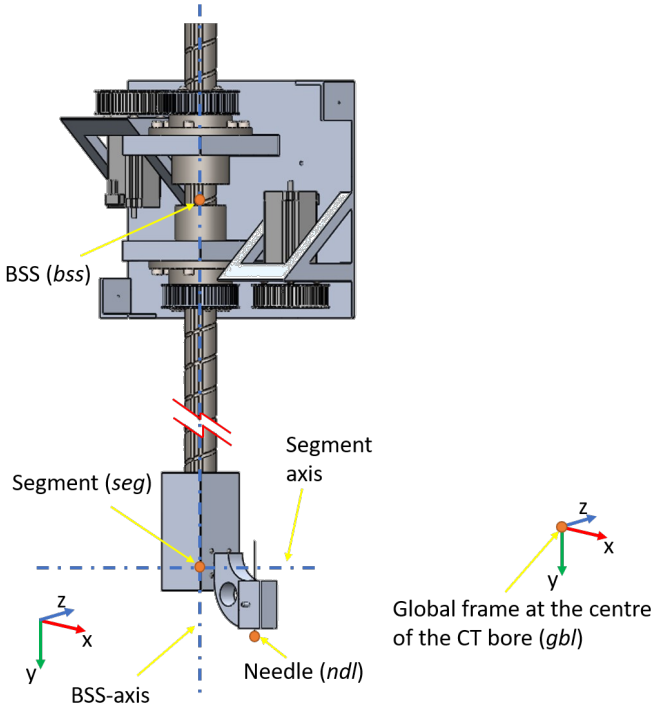

Figure 6.1

The first coordinate frame is fixed along the needle-axis and at the bottom of the needle holder. This frame is referred to as *ndl*. A Second frame is placed at intersection point of axis of rotation of BBS-shaft and the segment which is referred to as *seg*. Third frame is also placed along the axis of BSS-shaft and at centre of motor-mounting-plate which is referred as *bss*. The global coordinate is placed at the centre of the CT-bore and referred as *gbl*. Insertion point P_{ins}^{gbl} and tumour locations P_{tmr}^{gbl} are defined in the global frame.

$$\mathbf{H_{ndl}^{gbl}} = \mathbf{H_{bss}^{gbl}} \mathbf{H_{seg}^{bss}} \mathbf{H_{ndl}^{seg}} \tag{6.1}$$

Any point defined in the needle frame can be transformed to global frame and vice-versa using the matrix $\mathbf{H_{ndl}^{gbl}}$ which is given by the Equation 6.1. The HTM on the right hand side of Equation 6.1 are given below:

$$\mathbf{H_{bss}^{global}} = \begin{pmatrix} \mathbf{I_3} & P_{bss_O}^{gbl} \\ O_3^T & 1 \end{pmatrix} \tag{6.2}$$

$$\mathbf{H}^{\mathbf{bss}}_{\mathbf{seg}} = \begin{pmatrix} \mathbf{R_y} & P^{bss}_{seg_O} \\ O^T_3 & 1 \end{pmatrix} \tag{6.3}$$

$$\mathbf{H}^{\mathbf{seg}}_{\mathbf{needle}} = \begin{pmatrix} \mathbf{R_x} & P^{seg}_{ndl_O} \\ O^T_3 & 1 \end{pmatrix} \tag{6.4}$$

where, $P^{gbl}_{bss_O}$ is the offset of *bss* frame defined in *gbl* frame. Similarly, $P^{bss}_{seg_O}$ and $P^{seg}_{ndl_O}$ are offsets of *seg* and *ndl* frame defined in *bss* and *seg* frame respectively. $\mathbf{R_x}$ and $\mathbf{R_y}$ are rotation matrices along x and y respectively.

6.2 Inverse Kinematics

Different frames and respective HTM was developed and discussed in previous section. In this section, for given insertion point and tumour location the joint states are calculated.

Tumour $P^{gbl}_{tmr} = (x_{tmr}, y_{tmr}, z_{tmr})$ and insertion $P^{gbl}_{ins} = (x_{ins}, y_{ins}, z_{ins})$ points are identified in the *gbl* frame.

As a next step, relative angles between these two points are calculated using

$$\theta = \arctan\left(\frac{\sqrt{(x_{tmr} - x_{ins})^2 + (z_{tmr} - z_{ins})^2}}{y_{tmr} - y_{ins}}\right)$$

$$\Phi = \arctan\left(\frac{x_{tmr} - x_{ins}}{z_{tmr} - z_{ins}}\right)$$

The origin of *ndl* frame is transformed to *gbl* frame using

$$P^{gbl}_{ndl} = \mathbf{H}^{\mathbf{gbl}}_{\mathbf{ndl}}\Big|^{x=0}_{\theta,\Phi}{}_{y=0} \begin{pmatrix} 0 \\ 0 \\ 0 \\ 1 \end{pmatrix}$$

Now that both the points are defined in the global frame, relative distance d along the x, y and z is simply the difference between the points given by,

$$d = P^{gbl}_{tmr} - P^{gbl}_{ins}$$

A simple Graphical User Interface (GUI) is developed to take inputs from the user and calculate the joint states using the equations described above. A screenshot of the GUI is presented in the Figure 6.2.

For the given input points, θ, Φ and needle depth are calculated. Figure 6.3 shows the device in home position. Further, when the *Move* button is clicked in the GUI, the end-effector is positioned at the insertion point with needle guide oriented towards the target tumour. Figure 6.4 shows the final position of the end-effector and other joints. The position-time plot in Figure 6.5 shows the instantaneous position vs time for each of the joints. The joint velocity for the simulation are considered as follows: for X and Z axes, a linear velocity of $50\,\mathrm{mm\,s^{-1}}$ and for Y axis, a linear velocity of $25\,\mathrm{mm\,s^{-1}}$. For Φ and θ an angular velocity of $3.18\,\mathrm{rad\,s^{-1}}$ has been considered. These values are chosen considering the safety of the patient. Relatively slow motion of the end-effector also allows the physician to respond in-time and press the *emergency-stop* button in case of emergency.

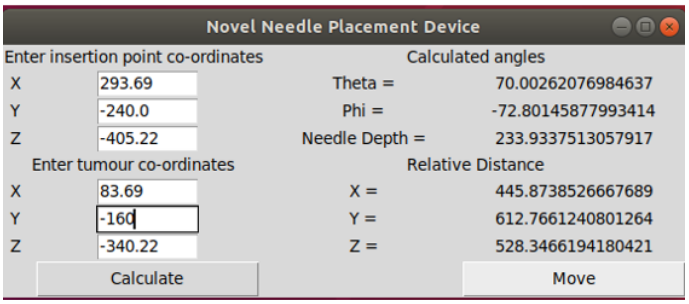

Figure 6.2: User interface to calculate joint states

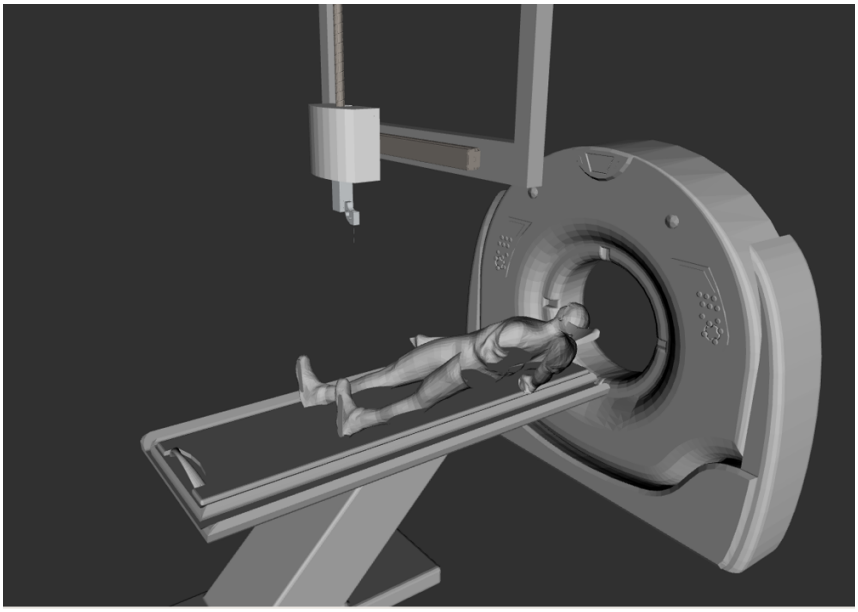

Figure 6.3: Device in home position

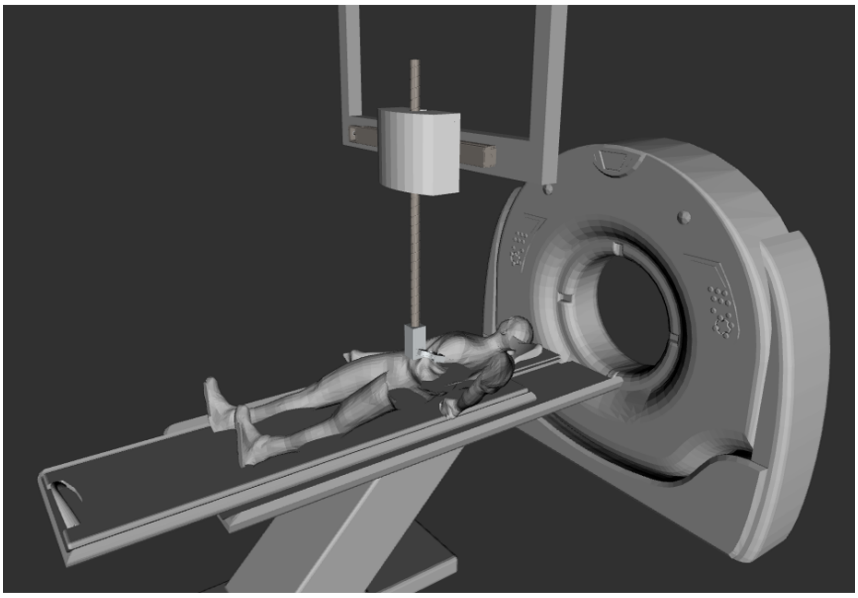

Figure 6.4: End-effector positioned at the insertion point

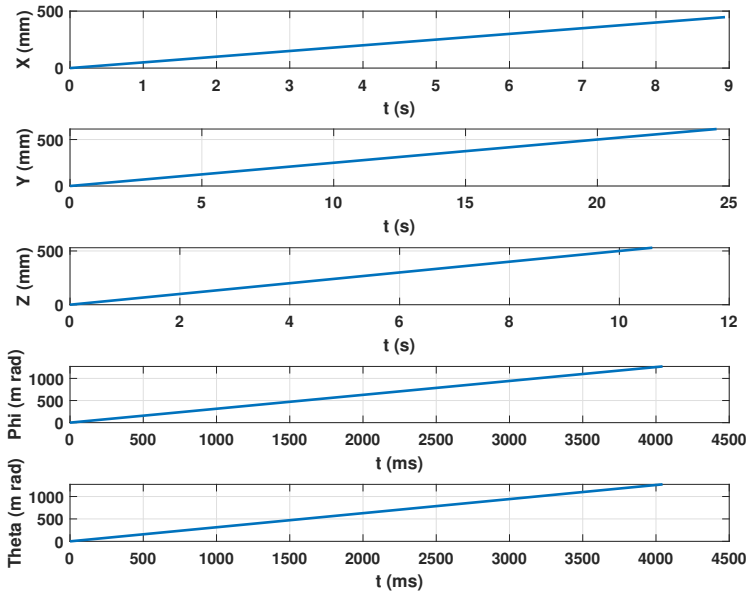

Figure 6.5: Position vs Time of all the joints

6.3 Error Analysis

In minimal intervention devices such as this novel system, the accuracy of needle placement plays a major role in the effectiveness of diagnosis or the surgery. Although there is no defined tolerance for accuracy of needle placement in general clinical practices, smaller misplacement results in higher precision in diagnosis and treatment. From Requirement 2, the maximum error in the system for placing a needle tip at a depth of 250 mm is 5 mm with a goal of of 2 mm. Various errors involved in the system are discussed this section.

The errors in the device can be broadly classified as error in *Position*, *Orientation* and *Stiffness*. Figure 6.6 defines errors involved in positioning and orientating the end-effector. Δ_px, Δ_py, Δ_pz corresponds to the error in position and $\Delta_o\phi$, $\Delta_o\theta$ corresponds to errors in Φ and θ respectively. Since the device is mounted to the ceiling, the translations along Δ_pz is performed by moving the table towards or away from the device. Therefore, accuracy of the system not only depends on the design of the device itself but also partly on the positioning accuracy of the CT machine. Typical value of positioning accuracy of the CT table is $\pm$500 µm (ImPACT, 2002).

Further, positioning accuracy of the LS-assembly is given to be 150 µm [ref. Table 5.5] and a backlash of 20 µm. Therefore, error along x, Δ_px is calculated as 170 µm. Due to the self weight of the ball-spline shaft and the segment holder assembly, the shaft always tends to be butted with the bottom surface of the screw. Also the ball-screw nut has angular contact arrangement. Therefore, the backlash along y can be assumed to be 0 and error in placement is limited by the resolution of motor and encoder. Assuming that the stepper motor is operated in full-step for linear motion, pitch over number of steps per rotation gives linear distance travelled per step. The selected motor consumes 400 steps per rotation and the pitch of BSS is 40 mm. Therefore, the Δ_py is found to be 100 µm. By operating the motor in micro-stepping, this error can be further reduced.

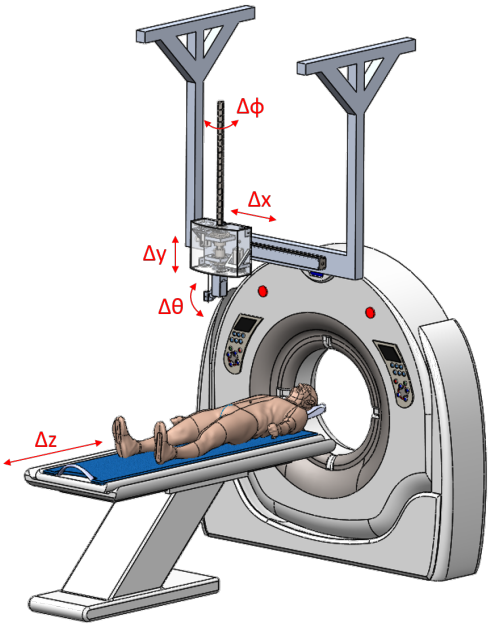

Figure 6.6: Error decomposition

The device offset calibration also plays a major role in overall accuracy of the system since these offsets are directly used in calculating homogeneous transformation matrices for inverse kinematics. Assuming that the offsets can be measured with an accuracy of 250 µm, error due to calibration can be considered as 250 µm along all the three axes.

The error in orientation is limited by the resolution of the motor in micro-stepping. Assuming the motor actuating both the rotary axes are actuated at 32 decimations per step for a motor with 400 steps per revolution, minimum angle that can be achieved is $\frac{360}{400\times32} = 0.028°$ $= 490.8 \times 10^{-6}$ rad. This translates to the needle tip located at 250 mm distance as 98.17 µm. However, the resolution of encoder is 5000 PPR. The minimum angle when quadrature encoding is employed is given by $\frac{360}{5000\times4} = 0.018°= 314 \times 10^{-6}$ rad . This translates to the needle tip located at 250 mm distance as 78.53 µm. Therefore, error at needle tip due to $\Delta_o\theta$ and $\Delta_o\Phi$ is considered to be 78.53 µm.

The device can be considered as a Cartesian robot, hence the errors along x,y and z linearly translates to the needle tip. The errors involved in the device are calculated at the needle tip and are tabulated in the Table 6.1. $\Delta_s x = \Delta_s z = \gamma_{bss}$ is calculated in Table 5.1. However, these errors are dependent on the value of Φ. If $\Phi = 0$ or π then maximum error occurs along Z direction and $\Delta_s z = 262$ µm and $\Delta_s x$ will be 0. $\Delta_s x$ will be maximum for $\Phi = \pm\frac{\pi}{2}$ where $\Delta_s z = 0$. Further, the deflection also depends on the value of θ and is maximum for $\theta = \frac{\pi}{2}$. Therefore, $\Delta_s x$ and $\Delta_s z$ can be written as,

$$\Delta_s x = \gamma_{bss} \cos\Phi \sin\theta$$

$$\Delta_s z = \gamma_{bss} \sin\Phi \sin\theta$$

Based on the stiffness requirement for the ceiling mount in Table 5.7, $\Delta_s y$ is calculated as 10 µm.

The errors involved in the system are tabulated in the Table 6.2. This includes error due to tumour registration and device calibration. Error max is calculated as sum of error along respective directions and euclidean of error due to orientation.

Table 6.1: Errors involved in the device calculated at the needle tip for a tumour located at 250 mm with respect to insertion point

Type	**Parameter**	**Error at needle tip** µm
Position	Δ_px	170
	Δ_py	100
Orientation	$\Delta_o\theta$	78.53
	$\Delta_o\Phi$	78.53
Stiffness	Δ_sx	0
	Δ_sy	10
	Δ_sz	262
Maximum Error	**Euclidean**	**442.18**

Table 6.2: Overall error in the system

Type	**Parameter**	**Error at needle tip** µm
Table translation error	Δ_pz	500
Error in the device	Euclidean	442.18
Device error including Δ_pz	**Euclidean**	**899.5**
Imaging (Arnolli, 2017)	Mean	810 ± 310.
Calibration	Δ_cx	250
	Δ_cy	250
	Δ_cz	250
Maximum Error	**Euclidean**	**2452.9**

6.3.1 Maximum error

Since the error along the Z axis is maximum, the maximum error occurs when the needle is inserted parallel to the Z axis corresponding to $\theta = \frac{\pi}{2}$. Since this is not a practical scenario, a special case is considered. Consider the scenario presented in Figure 5.14 where $\Phi = 0$ and $\theta = \frac{\pi}{3}$. Further, let the motor mounting plate be placed exactly at the centre of the beam such that the deflection of the beam is maximum. Let BSS shaft be extended to its maximum length and a force of 25 N is exerted on the needle. Figure 6.7 illustrates intended needle path and actual needle path along with intended tumour position and actual tumour position. Various errors involved are also depicted. This scenario presents the case where maximum error occurs.

6.4 Risk Analysis

The risk and failure analysis plays a very important role in medical devices such as this novel needle placement system. Various types of failures can occur in the system including but not limited to failure of parts and operations.

6.4.1 Failure of parts

The weakest link in the system is the belt driving the ball-spline shaft. Estimated weight of the BSS shaft including the end-effector assembly is approximately 5 kg. Considering acceleration due to gravity $g = 9.8\,\mathrm{m\,s^{-2}}$, an impulsive force of 49 N is experienced by the patient in case of failure of belt which can lead to catastrophic injury. Keeping this in mind, a belt with a steel core wire is selected. Although due to the steel reinforcement the chances of failure is low, breakage can occur if the belt is over-stressed. Since the part is concealed,

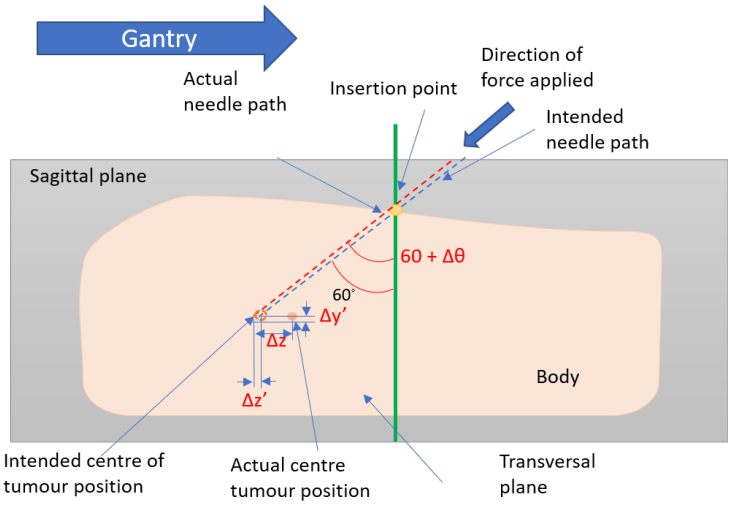

Figure 6.7: Illustration of scenario for max error

indication or detection of failure is virtually impossible. Hence, as a precautionary measure, annual preventive maintenance has to be conducted and the part has to be replaced.

Redundant Sensor

A second source of feedback about the distance of patient from the end-effector should be employed to ensure that the end-effector does not cause accidental injury to the patient. This can be achieved using a laser based distance measuring system which can be attached to the ceiling mount. The software should also be provided with a control switch and the BSS should be lowered in close supervision. The physician should be able to abort the procedure with an *emergency-stop* switch in case of any abrupt motion of the BSS shaft.

6.4.2 Failure of operation

Many a time accidents happen due to human error. One such error could be moving the device while the needle is still attached to the system. Therefore it is important to double-check and ensure that the needle is disengaged from the device before actuating the motors. An optical sensor can be strategically placed on the segment to check if the needle is disengaged before moving the joints. Further the motors should be actuated only after the physician visually confirms and enables the actuation.

6.5 Discussions

6.5.1 Manufacturing tolerances

Manufacturing tolerance also play a role in overall accuracy of the system. from the Table 6.2, the total error in the system is found to be 2.5 mm. By manufacturing all the custom part and by ensuring that the overall tolerances is 10% of the system error, the maximum error will be 2.7 mm. However, since there is an error budget of 5 mm, one could choose to manufacture at lower tolerances and at a lower manufacturing cost.

6.6 Conclusion

A brief study on kinematic simulation is performed in this chapter. Forward and inverse kinematics are implemented and error analysis is performed. A case study is done for a scenario where the error can be maximum and the maximum error is found to be 2.5 mm.

7 Verification

A verification of design by analysis against each requirement and brief comparison of the novel device with DEMCON NPS against some parameters are presented in this Chapter along with the limitations of the novel device.

7.1 Verification of Design by Analysis

Each of the requirements stated in Chapter 3 is verified by analysis in this section.

Requirement 1: *The system shall be capable of repositioning the end effector to a new entry point with no radiation exposure to the patient.*

- **Analysis:** From the work-flow presented in the Section 4.1.4, it is clear that no extra scans are needed to perform additional needle placement. Furthermore, the device registration scan is also eliminated.
- **Verification Result:** Pass.
- **Comment:** One of the important feature that was lacking in DEMCON NPS was the ability to reposition the device to a different insertion point located elsewhere in the thorax and abdomen region. This problem is solved with the novel device.

Requirement 2: *The system shall be able to place the needle tip at the target within maximum error of* 5 mm *for a target located at a depth of* 250 mm *with a design goal of* 2 mm.

- **Analysis:** From the Section 6.3, the calculated maximum error of the system is expected to be 2.5 mm. Thus, the specification meets the requirement and is closer to the design goal.
- **Verification Result:** Pass.
- **Comment:** From Arnolli et al. (2018), it can be found that the mean error in needle placement at a depth of 250 mm for DEMCON NPS is claimed to be 2.6 ± 0.7mm. However, a maximum error of 9.2 ± 4.0mm at a depth of 94.8 ± 31.7mm was reported by Heerink et al. (2019). The maximum error expected at depth of 250 mm for the novel device based on theoretical calculations is found to be 2.5 mm.

Requirement 3: *The system shall support placement of insertion point in thorax and abdomen region.*

- **Analysis:** Based on the stroke length of the LS assembly and the maximum extension of the BSS, all points in the abdomen and thorax region can be reached.
- **Verification Result:** Pass.

Requirement 4: *The system shall be applicable to needle paths both coincident with and oblique to the transversal plane up to* 90°.

- **Analysis:** Since no mechanical constraints on axis of θ has been introduced in the design, all angles up to 90° with respect to transversal or sagittal plane can be achieved.

- **Verification Result:** Pass
- **Comment:** From the Figure 7.1 it can be found that the maximum angle that can be achieved by the NPS is 45° with respect to normal. However, the Orientation Module (OM) of the NPS can be tilted to reach any point located beyond 45°, thus changing the orientation of the reachable region. Since the NPS is a table-mounted device, the OM cannot be adjusted beyond a certain degree (depending on the patient size) due to: (a) the device will start to hit the patient and (b) mechanical constraints. However, in the novel device, since there is no mechanical limitation on θ, and the end-effector can assume any angle including 90° with respect to transversal or sagittal plane.

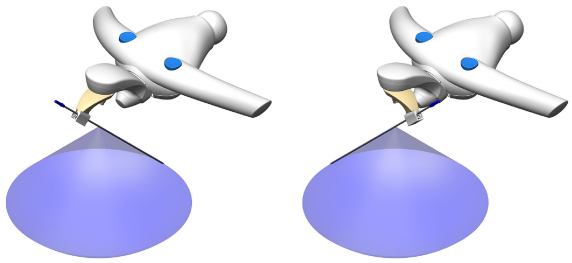

(A) Needle 45° to the back. (B) Needle 45° to the right.

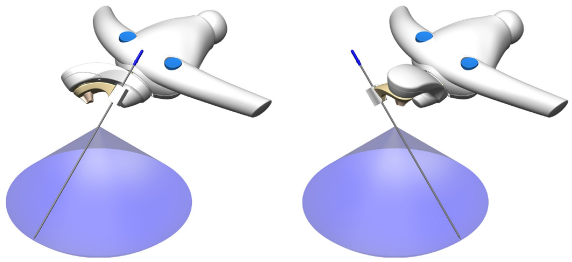

(C) Needle 45° to the front. (D) Needle 45° to the left.

Figure 7.1: Cone formed by the DEMCON NPS adapted from Arnolli (2017)

Requirement 5: *The system shall support needles used for biopsy and ablation with diameters ranging between 14 - 23 gauge.*

- **Analysis:** Design of needle holder ensures usage of all possible needle sizes in the device.
- **Verification Result:** Pass

Requirement 6: *The system shall support a sterile operating environment.*

- **Analysis:** The segment assembly can be easily detached from the device by unscrewing the set-screw for sterilization. Furthermore, a disposable sterile bag can be wrapped around the segment and the segment-holder assembly to ensure sterility of the field is not violated.
- **Verification Result:** Pass

Requirement 7: *The system design shall avoid hindrance to the physician by preventing the presence of system components between the patient and the physician.*

- **Analysis:** Since the device is moved back to home position (refer Figure 6.3) immediately after inserting the needle, hindrance to the physician is minimum. Furthermore, the device can be positioned at the centre of the LS-assembly to ensure that the accidents to physicians are avoided while performing clinical procedure.
- **Verification Result:** Pass

7.2 Limitations

The limitation of a *ceiling-mounted BSS-actuated* device is that the length of the BSS shaft has to be modified and the height of the ceiling mount with respect to floor has to adjusted depending on the CT room dimensions. This implies that the length of the BSS shaft cannot be standardized and has to be custom designed for each case. Further, since the device is fixed to the ceiling, the flexibility of the device is lost. That is in case of the NPS, since it is a table mounted device, it can be attached to any CT table. However, a ceiling mounted device cannot be relocated easily. Furthermore, the physician should intuitively trust the needle path during the needle-placement since there is no real-time feedback about the location of the needle tip.

8 Conclusions and Recommendations

8.1 Conclusions

With minimal invasive surgeries getting popular by day for clinical procedures like biopsy and ablation, various image (CT, MRI, US) guided devices have been developed which aids placement of the needle accurately at the target tumour. These devices range from simple passive mechanisms to articulated robots. The Needle Placement System developed by DEMCON is such a device which aids in placement of the needle at the target accurately. However, while performing Irreversible Electroporation, Microwave Ablation or cryo-ablation; multiple needles have to be inserted. This requires additional scans to be performed. As a result, the patient is exposed to hazardous ionizing radiation which can cause radiation induced cancer in the patient. Hence, this brings forth the following question, *How can the insertion point be repositioned without performing extra scans, while keeping the accuracy and precision of the new insertion the same as that of the initial insertion?*.

Different needle placement devices ranging from a simple gravity aided passive device to sophisticated robots are discussed and the working principle of each kind of mechanism is studied. The floor-mounted category was further explored due to advantage of eliminating an extra scan when a repositioning of insertion point or additional needle-placement is required. This concept was further developed and a new category namely *ceiling mounted* devices that assist in percutaneous needle-placement was developed as a conceptual solution. The floor-mounted devices are bulky and occupy more space next to CT bed creating hindrance to the physician to access the patient. The hindrance to the physician is significantly reduced by mounting the device to the ceiling. Furthermore, once the needle is inserted in the patient, it is disengaged from the device and the device is moved to home position. Thus, the device shall not cause any hindrance to the physician in conducting diagnostic or therapeutic procedure. A workflow describing the elimination of an extra scan has been illustrated in Section 4.1.4. Therefore, with the novel device, n needle-placements require $n+1$ CT-scans. Whereas DEMCON NPS requires $2n+1$ CT-scans, assuming gross placement of the needle-guide for subsequent insertions is performed based on initial scan data.

A detailed mechanical design of all the parts of the device has been discussed. While some parts can be bought directly off-the-shelf, some require modification after procuring the parts. Some custom-made parts were also designed. The BSS shaft and the end-effector contribute significantly to overall weight of the device. Since BSS shaft consists of a ball-screw, the friction is minimal and breakage of belt pose a risk to the patient as the BSS shaft can slide and drop on the patient in which case, the patient might experience an impulsive force of 49 N which may lead to catastrophic injury. Therefore, a timing belt with steel-reinforcement must be employed and a preventive maintenance should be conducted to replace the belt periodically. Kinematic simulations were performed and position vs time plot has been presented. Error and risk analysis is carried out and maximum error in the system is found to be <2.5 mm for a tumour located at 250 mm depth.

8.2 Recommendations

The novel device has been developed from engineering perspective and therefore as a first recommendation, the concept and the design solution has to be discussed in detail with the physicians and a feasibility study should be performed. A mock device developed using rapid prototyping can be used to conduct a feasibility study. Design maybe modified

accordingly to adapt the device to the room dimensions such that minimum device-to-floor distance is maintained. Further, a fully functional prototype maybe developed to verify actual performance by test and first-hand experience from the physicians maybe be obtained by conducting a phantom study. As a next step, the system should be integrated with a GUI which should be capable of acquiring images from CT and also controlling the motion of CT bed. Further, since all the joints are computer controlled, an active respiratory motion compensation can be implemented. Furthermore, the needle-placement can also be automated by designing a precisely controlled device capable of inserting the needle to the required depth which can be attached to the segment replacing the needle holder. Although this reduces human error in needle-placement, extensive validation is required since the needle will be inserted without physician's intervention.

A Concept: Table mounted; fixed orientation

One of the solutions to overcome the requirement of needing a device registration scan is to mount the device in a fixed orientation as illustrated in the Figure A.1.

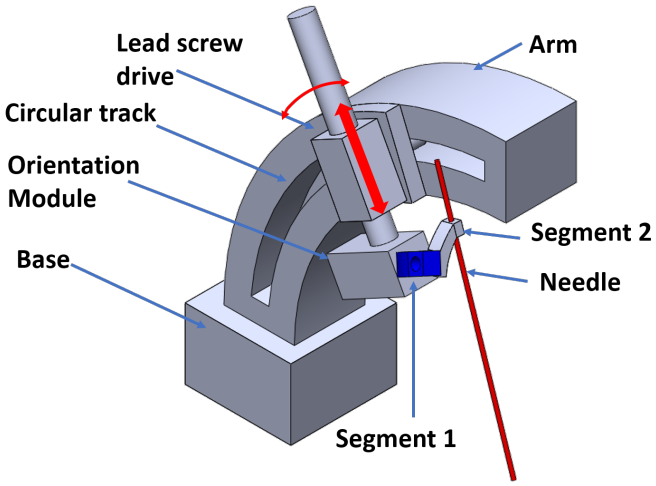

Figure A.1: Illustration of Concept 1

The device consists of an arm, which is mounted to the CT table. The arm consists a circular track to which the Orientation Module (OM) of the NPS is attached via a screw drive. The screw drive provides translation degree of freedom to the OM to move towards and away from the patient. The OM of the NPS further consists two segments and the needle guide is attached to the second segment. The OM of the NPS and both the segments are actuated by motors. The device has a total of 4-DOFs

Further, the device is mounted on the CT table and radiopaque grid is placed on the patient and initial scan is performed. The insertion point is identified and the grid number is noted down. The table is translated to align the transversal plane containing the insertion point deduced from the image with the laser beam projecting from the gantry. The intersection of the grid containing the insertion point and the laser beam is marked. The device is manually placed at the insertion point on the patient. Initial scan images are analysed and the target is selected. Relative angles between the target and the insertion point are calculated and the segments are actuated. CT table is translated away from the gantry and the needle is inserted. A verification scan is performed.

For repositioning the insertion point, the new insertion point is selected from the initial scan images. Relative distances between the new point and the initial point is calculated and the device is repositioned automatically. However, if the new insertion point is not in the same plane as that of the device, since device itself is constrained to move along the table, the physician has to manually move the device to the new insertion point. Furthermore, since the device enters the imaging field along with the patient, the size and shape of the device are limited, also the parts and components needs to be made of CT compatible material.

B Cost Budgeting

Cost of the device is an important parameter while designing any system. An approximate cost estimate of the device and a bill of materials is tabulated in Table B.1. Fasteners and springs are excluded from the list.

Table B.1: Cost estimates

Part	Part number	Manufacturer	Rate (€)	Quantity	Price (€)
Ceiling support	-	-	500	1	500
Segment	-	Custom	250	1	250
Needle holder	-	Custom	150	1	150
Needle holder clip	-	Custom	20	1	20
Plungers	-	Custom	50	2	100
Needle holder plate	-	Custom	50	1	50
Segment Holder	-	Custom	300	1	300
Segment Enclosure	-	Custom	20	1	20
Enclosure	-	Custom	200	1	200
Motor mounting plate (assembly)	-	Custom	1500	1	1500
Ball Spline assembly	BNS4040 + 1200L	THK	1500 (per meter)	1	1800
LS-Assembly	KR45H10D+940LH0-100A	THK	2000	1	2000
LS-Motor plate	-	Custom	50	1	50
Pulley	40T10/30-2	B&B	30	4	120
Pulley (adaptation)	-	Custom	30	4	120
Belt	TTBU900T10250	Misumi	60	2	120
Motors	ST4118M0406-B	Nanotec	25	1	25
	ST6018D4508-B	Nanotec	114	2	228
	SC3518L1204-B	Nanotec	50	1	50
Encoders	NT03-05-206(6.35mm)	Nanotec	70	4	280
Brakes	BKE-2,0-6,35	Nanotec	95	2	190
Total				34	**8073**

Bibliography

Maarten M Arnolli, Nevan C Hanumara, Michel Franken, Dannis M Brouwer, and Ivo AMJ Broeders. An overview of systems for ct-and mri-guided percutaneous needle placement in the thorax and abdomen. *The International Journal of Medical Robotics and Computer Assisted Surgery*, 11(4):458–475, 2015.

Maarten M Arnolli, Martijn Buijze, Michel Franken, Ivo AMJ Broeders, and Dannis M Brouwer. A precision system for computed tomography-guided needle placement in the thorax and abdomen—technical design and performance analysis. *Journal of medical devices*, 12(2), 2018.

Maarten Menno Arnolli. *Development of a precision system for image-guided needle placement*. PhD thesis, University of Twente, Enschede, The Netherlands, 2017. URL https://doi.org/10.3990/1.9789036543323.

Lukas P Beyer, Benedikt Pregler, Christoph Nießen, Andreas Schicho, Michael Haimerl, Ernst Michael Jung, Christian Stroszczynski, and Philipp Wiggermann. Stereotactically-navigated percutaneous irreversible electroporation (ire) compared to conventional ire: a prospective trial. *PeerJ*, 4:e2277, 2016.

José Cabieses. Man, 2014. URL https://grabcad.com/library/man-1/details?folder_id=367271. CAD model of a man.

CAS-ONE. Cascination cas-one ir, 2020. URL https://www.cascination.com/products/cas_one_ir.

GuideLines-CT-Biopsy-Grid. Medical-imaging-systems, 2020.

Wouter J Heerink, Simeon JS Ruiter, Jan Pieter Pennings, Benno Lansdorp, Rozemarijn Vliegenthart, Matthijs Oudkerk, and Koert P de Jong. Robotic versus freehand needle positioning in ct-guided ablation of liver tumors: a randomized controlled trial. *Radiology*, 290(3):826–832, 2019.

ImPACT. Single slice ct scanner comparison report, 2002. URL http://www.impactscan.org/reports/full/MDA02020.pdf. Compiled and prepared by members of the ImPACT group.

INRAD. Accuplace® drace stereotaxic needle guide, 2020. URL https://www.inradinc.com/accuplace-drace-stereotaxic-needle-guide/.

Ahmet Kandemir. Medical ct, 2015. URL https://grabcad.com/library/medical-ct-1. CAD model of a CT.

Joachim Kettenbach, Levent Kara, Grzegorz Toporek, Martin Fuerst, and Gernot Kronreif. A robotic needle-positioning and guidance system for ct-guided puncture: ex vivo results. *Minimally invasive therapy & allied technologies*, 23(5):271–278, 2014.

Yilun Koethe, Sheng Xu, Gnanasekar Velusamy, Bradford J Wood, and Aradhana M Venkatesan. Accuracy and efficacy of percutaneous biopsy and ablation using robotic assistance under computed tomography guidance: a phantom study. *European radiology*, 24(3):723–730, 2014.

Maarten Kroes. *Impact of laser guidance in image-guided needle interventions*. PhD thesis, Radboud University, The Netherlands, 2017. URL https://hdl.handle.net/2066/178236.

Maarten W Kroes, Wendy MH Busser, Jurgen J Fütterer, Mark J Arntz, Caroline MM Janssen, Yvonne L Hoogeveen, Frank de Lange, and Leo J Schultze Kool. Assessment of needle guidance devices for their potential to reduce fluoroscopy time and operator hand dose during c-arm cone-beam computed tomography–guided needle interventions. *Journal of*

Vascular and Interventional Radiology, 24(6):901–906, 2013.

Anders Magnusson, Eva Radecka, Maria Lönnemark, and Hans Raland. Computed-tomography-guided punctures using a new guidance device. *Acta Radiologica*, 46(5):505–509, 2005.

BJ McParland. A study of patient radiation doses in interventional radiological procedures. *The British journal of radiology*, 71(842):175–185, 1998.

Medtronic. Axiem™ electromagnetic technology for stealthstation® navigation system, 2009. URL https://www.medtronic.com/. Procedure guide.

Georgi Minchev, Gernot Kronreif, Mauricio Martínez-Moreno, Christian Dorfer, Alexander Micko, Aygül Mert, Barbara Kiesel, Georg Widhalm, Engelbert Knosp, and Stefan Wolfsberger. A novel miniature robotic guidance device for stereotactic neurosurgical interventions: preliminary experience with the isys1 robot. *Journal of neurosurgery*, 126(3):985–996, 2017.

Carsten Moser, Jan Becker, Martin Deli, Martin Busch, Marc Boehme, and Dietrich HW Groenemeyer. A novel laser navigation system reduces radiation exposure and improves accuracy and workflow of ct-guided spinal interventions: a prospective, randomized, controlled, clinical trial in comparison to conventional freehand puncture. *European journal of radiology*, 82(4):627–632, 2013.

Donald L Myers. Imaging services design guide, 2020. URL https://www.cfm.va.gov/til/dGuide/dgImaging.pdf.

NAV3i. Stryker nav3i, 2020. URL https://www.stryker.com/us/en/navigation/products/nav3i.html.

NDI-Medical. Aurora, 2020. URL https://www.ndigital.com/medical/products/aurora.

NeoRad-SimpliCT. Neorad navigation solutions simplict, 2020. URL https://www.neorad.no.

Tobias Penzkofer, Philipp Bruners, Peter Isfort, Felix Schoth, Rolf W Günther, Thomas Schmitz-Rode, and Andreas H Mahnken. Free-hand ct-based electromagnetically guided interventions: accuracy, efficiency and dose usage. *Minimally Invasive Therapy & Allied Technologies*, 20(4):226–233, 2011.

Perfint-Healthcare. Perfint maxio and perfint robio, 2020. URL http://www.perfinthealthcare.com/.

Diwakar Shastri. Development of concept for low-cost needle positioning system. [Internship report; Company: Demcon Advanced Mechatronics B. V., Enschede, Netherlands], December 2019.

Aaron Sodickson, Pieter F Baeyens, Katherine P Andriole, Luciano M Prevedello, Richard D Nawfel, Richard Hanson, and Ramin Khorasani. Recurrent ct, cumulative radiation exposure, and associated radiation-induced cancer risks from ct of adults. *Radiology*, 251(1):175–184, 2009.

THK. Lm guide actuator kr, 2011. URL https://tech.thk.com/upload/catalog_claim/pdf/cat_kr_en.pdf. Datasheet, Document No: 209-8E.

THK. Selecting a preload, 2020. URL https://tech.thk.com/en/products/pdf/en_a03_030.pdf. Datasheet, Document No: 513E.

D Wallach, G Toporek, Stefan Weber, Reto Bale, and Gerlig Widmann. Comparison of freehand-navigated and aiming device-navigated targeting of liver lesions. *The International Journal of Medical Robotics and Computer Assisted Surgery*, 10(1):35–43, 2014.

Shane A Wells, J Louis Hinshaw, Meghan G Lubner, Timothy J Ziemlewicz, Christopher L Brace, and Fred T Lee. Liver ablation: best practice. *Radiologic Clinics*, 53(5):933–971, 2015.

XACT-Robotics. Technology xact robotics™, 2020. URL https://xactrobotics.com/technology/.